Measurement of NO_x and NO_y with a thermal dissociation cavity ring-down spectrometer (TD-CRDS): Instrument characterisation and first deployment.

Nils Friedrich[1], Ivan Tadic[1], Jan Schuladen[1], James Brooks[2], Eoghan Darbyshire[2], Frank Drewnick[1], Horst Fischer[1], Jos Lelieveld[1], John N. Crowley[1]

[1]Atmospheric Chemistry Department, Max Planck Institute for Chemistry, Mainz, 55128, Germany
[2]Centre of Atmospheric Science, University of Manchester, Manchester, UK

Correspondence to: John N. Crowley (john.crowley@mpic.de)

Abstract. We present a newly constructed, two channel Thermal Dissociation Cavity Ring-Down Spectrometer (TD-CRDS) for the detection of NO_x (NO + NO_2), NO_y (NO_x + HNO_3 + RO_2NO_2 + N_2O_5 etc.), NO_z (NO_y - NO_x) and particulate nitrate (pNit). NO_y-containing trace gases are detected as NO_2 by CRDS at 405 nm following sampling through inlets at ambient temperature (NO_x), or at 850 °C (NO_y). In both cases, O_3 was added to the air sample directly upstream of the cavities to convert NO (either ambient, or formed in the 850 °C oven) to NO_2. An activated carbon denuder was used to remove gas-phase components of NO_y when sampling pNit. Detection limits (1 minute averaging) for NO_x, NO_y and NO_z are 98, 51 and 110 pptv, respectively. The total measurement uncertainties (at 50% RH) in the NO_x and NO_y channels are 11% + 10 pptv and 16% + 14 pptv for NO_z, respectively. Thermograms of various NO_z species (peroxyacetyl nitrate, isopropyl nitrate, and HNO_3) confirm stoichiometric conversion to NO_2 (and / or NO) at the oven temperature and rule out significant interferences from NH_3 detection or radical recombination reactions under ambient conditions. While fulfilling the requirement of high particle transmission and essentially complete removal of reactive nitrogen under dry conditions, the denuder suffered from NO_x breakthrough and memory effects (i.e. release of stored NO_y) under humid conditions.

NO_x measurements obtained from a ship sailing through the Red Sea, Indian Ocean and Arabian Gulf (NO_x levels from < 20 pptv to 25 ppbv) were in excellent agreement with those taken by a chemiluminescence detector of NO and NO_2. A dataset exploring variations in the NO_z to NO_y ratio (maximum value of 0.6) of air in a region (Mainz, Germany) with strong urban influence was measured over a one-week period in winter.

1 Introduction

1.1 Atmospheric NO_x and NO_y

Total reactive nitrogen NO_y (= NO_x + NO_z) consists of nitrogen oxide NO, nitrogen dioxide NO_2 (NO + NO_2 = NO_x) and their reservoir species NO_z (NO_3 + $2N_2O_5$ + HNO_3 + HONO + $RONO_2$ + RO_2NO_2 + $XONO_2$ + XNO_2 + pNit), where X is a halogen

5 atom. HCN and NH_3 are generally not considered to be components of NO_y (Logan, 1983).

Formation of both peroxy nitrates (RO_2NO_2, PNs) and alkyl nitrates ($RONO_2$, ANs) require the presence of organic peroxy radicals (RO_2), which are formed in the reaction of OH radicals with volatile organic compounds (VOCs) and oxygen (reaction R1). RO_2 radicals react subsequently with NO_2 or NO to form peroxy-nitrates (RO_2NO_2, PNs) or alkyl-nitrates ($RONO_2$, ANs, reactions R2 and R3). Reaction R3 competes against the formation of an alkoxy radical (RO) and the oxidation of NO to NO_2

10 (reaction R4), which consumes the dominant fraction of RO_2. The branching ratio between these two pathways depends on atmospheric conditions such as pressure and temperature and on the structure and length of the organic backbone (Lightfoot et al., 1992). HNO_3 is produced mainly via the reaction of NO_2 with OH (reaction R5).

$$OH + RH + O_2 \rightarrow RO_2 + H_2O \tag{R1}$$

$$RO_2 + NO_2 + M \rightarrow RO_2NO_2 + M \tag{R2}$$

15 $$RO_2 + NO + M \rightarrow RONO_2 + M \tag{R3}$$

$$RO_2 + NO \rightarrow RO + NO_2 \tag{R4}$$

$$OH + NO_2 + M \rightarrow HNO_3 + M \tag{R5}$$
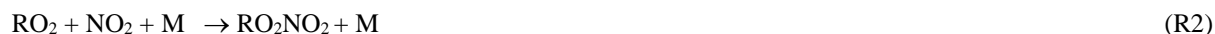
The lifetimes of peroxy nitrates in the low troposphere are mainly governed by the temperature. PNs with an additional acyl group (PANs), such as peroxyacetyl nitrate (PAN), are generally more stable than PNs without an acyl group (e.g. pernitric

20 acid HO_2NO_2), which are observed only in cold regions (Slusher et al., 2002). Thus, of the peroxy nitrates only PANs are considered able to act as transportable reservoirs for NO_x. At higher altitudes in the troposphere (above ca. 7 km) photolysis becomes the most important loss process for PAN, while the reaction with OH is negligible in the entire troposphere (Talukdar et al., 1995).

The absence of photolysis reactions and low levels of the OH radical at nighttime open alternative pathways to formation of

25 NO_z species. NO_2 is oxidised by O_3 to produce the nitrate radical NO_3, which exists in thermal equilibrium with N_2O_5 (reactions R6 and R7). The reaction of NO_3 with hydrocarbons represents a nighttime source of alkyl nitrates (reaction R8), N_2O_5 can be hydrolysed on aqueous aerosol resulting in the formation of HNO_3 (reaction R9) and $ClNO_2$ (reaction R10) if particulate chloride is available (Finlayson-Pitts et al., 1989).

$$NO_2 + O_3 \rightarrow NO_3 + O_2 \tag{R6}$$

30 $$NO_3 + NO_2 \rightleftharpoons N_2O_5 \tag{R7}$$

$$NO_3 + RH \rightarrow RONO_2 \tag{R8}$$

$$N_2O_5 + H_2O \rightarrow 2 HNO_3 \tag{R9}$$

$$N_2O_5 + Cl^- \quad \rightarrow ClNO_2 + NO_3^- \quad\quad\quad\quad (R10)$$

Nitric acid formation via the reaction of NO_2 and OH (reaction R5), followed by wet or dry deposition of HNO_3, is considered to be the dominant daytime loss process for atmospheric NO_x (Roberts, 1990), though the reduction of NO_x may result in an increasingly important role for organic nitrates, e.g. in the USA (Romer Present et al., 2019). As some organic nitrates are

5 longer lived than HNO_3, the atmospheric transport of NO_x to remote locations would lead to a more even distribution of NO_x, instead of hotspots in polluted regions close to emission sources. Atmospheric removal processes for ANs include oxidation by OH or O_3 (which may lead to a loss of the nitrate functionality), deposition to the earth's surface and photolysis. Additionally, partitioning into the aerosol phase is possible for large and multifunctional ANs (Perring et al., 2013). Alkyl-nitrates possessing no further functionality (e.g. double bonds or hydroxyl groups) can be unreactive and have long lifetimes

10 (Talukdar et al., 1997). On the global average, $RONO_2$ has a lifetime of close to 3 hours (2.6 – 3 hours) with ~ 30% being lost by hydrolysis (Zare et al., 2018).

The formation of NO_z in the lower atmosphere reduces the NO_x lifetime and the partitioning of NO_y into NO_x and NO_z can provide information about the chemical history of an air-mass (Day et al., 2002; Wild et al., 2014). In regions impacted by biogenic emissions, the sources and sinks of ANs account for a large fraction of NO_x lost both during the day and night and

15 thus control the lifetime of NO_x (Romer et al., 2016; Sobanski et al., 2017).

Laboratory experiments have shown that particulate nitrates (pNit) are formed at high yields in the atmospheric degradation of terpenoids in the presence of NO_x and play an important role in the formation and growth of secondary organic aerosol (SOA)(Ng et al., 2017; IUPAC, 2019). This has been confirmed in field studies, which provide evidence for the partitioning of organic nitrate to the aerosol phase both during day- and nighttime (Rollins et al., 2012; Fry et al., 2013; Palm et al., 2017)

20 with formation of highly functionalised molecules and large contributions (up to 25%) of particulate organic nitrates to the total aerosol mass (Xu et al., 2015; Lee et al., 2016; Huang et al., 2019).

1.2 Detection of NO_x

Present day methods for the detection of NO and NO_2 are Chemiluminescence (CLD), Differential Optical Absorption Spectroscopy (DOAS), Laser Induced Fluorescence (LIF) and Cavity Ring-Down Spectroscopy (CRDS). A description and

25 inter-comparison of these methods is given in Fuchs et al. (2010) and we restrict the following discussion to an outline of the basic principles. The CLD method detects NO by chemiluminescent emission in its reaction with O_3; detection of ambient NO_2 by CLD follows its catalytic or photolytic conversion to NO. The best CLD devices have detection limits for NO and NO_2 in single-digit pptv range (Beygi et al., 2011; Reed et al., 2016; Tadic et al., 2019). Detection of NO_2 via LIF involves photo-excitation in its visible absorption band at wavelengths > 400 nm and detection of fluorescent emission at wavelengths

30 > 600 nm, with detection limits of the order of pptv achieved for an integration time of a few seconds (Day et al., 2002; Javed et al., 2019). The structured spectrum of NO_2 between $\approx$ 400 and 600 nm is used to detect light absorption by ambient NO_2 by DOAS, using either broad-band light sources (long-path DOAS, over a few km pathlength) or natural sunlight (Platt et al., 1979; Leser et al., 2003; Pohler et al., 2010; Merten et al., 2011).

The CRDS detection method for NO_2 also utilises its visible absorption spectrum, high sensitivity being achieved by achieving very long pathlengths for optical extinction in an optical resonator (see Sect. 2.1). Limits of detection for NO_2 with CRDS of < 20 pptv in 1 second integration time have been reported (Wild et al., 2014). NO can be detected (as NO_2) following its reaction with O_3 (R6).

1.3 Detection of NO_y

The first NO_y measurements were based on the conversion of all reactive nitrogen trace gases (apart from NO) to NO on catalytic metal surfaces of gold at ~ 300-320 °C or of molybdenum oxide at ~ 350-400 °C (Fahey et al., 1985; Williams et al., 1998), with subsequent CLD detection of NO. Au converters were designed to exclude particulate nitrates, while MoO setups aimed at a response towards pNit (Williams et al., 1998). In recent years, the thermal decomposition of NO_z to NO_2 has been used to detect total NO_z using inlets held at temperatures high enough (> 650-700 °C) to thermally dissociate the most strongly bound reactive nitrogen trace-gas, HNO_3, to NO_2 (Day et al., 2002; Rosen et al., 2004; Wooldridge et al., 2010; Perring et al., 2013; Wild et al., 2014) and/or using multiple inlets at intermediate temperatures (Paul et al., 2009; Paul and Osthoff, 2010; Sadanaga et al., 2016; Sobanski et al., 2016; Thieser et al., 2016). Subsequent to thermal decomposition, the NO_2 product can be detected using LIF (Day et al., 2002; Day et al., 2003; Rosen et al., 2004; Murphy et al., 2006; Wooldridge et al., 2010) or cavity enhanced absorption spectroscopy (Paul et al., 2009; Wild et al., 2014; Sadanaga et al., 2016; Sobanski et al., 2016; Thieser et al., 2016). These techniques are impacted to various degrees by secondary reactions at high temperatures including loss of NO_2 via recombination with α-carbonyl peroxy radicals or reaction with O-atoms (formed by the pyrolysis of ambient O_3) and the generation of extra NO_2 from the oxidation of NO via reactions with peroxy radicals (Day et al., 2002; Sobanski et al., 2016; Thieser et al., 2016; Womack et al., 2016). Measures to reduce potential measurement artefacts and avoid excessive data correction include operation at low pressures (Day et al., 2002; Womack et al., 2016) and addition of surfaces to scavenge peroxy radicals (Sobanski et al., 2016). Nonetheless, data correction may still be necessary, which may involve laboratory characterisation and chemical simulation of the chemical reactions within the heated inlet (Sobanski et al., 2016; Thieser et al., 2016).

In this paper we present a two-channel TD-CRDS instrument for detection of NO_x, NO_y, NO_z and pNit which overcomes these limitations.

2 Experimental

Our TD-CRDS instrument consists of two identically constructed cavities to monitor NO_2 at 405 nm which are largely unchanged compared to those described by Thieser et al. (2016). In the present set-up, the two cavities are connected to three different inlets. One cavity monitors NO_x via an inlet at ambient temperature, the second samples air via either of two heated inlets (one equipped with a denuder, see below) and thereby monitors either NO_y or particle nitrate. A schematic diagram (not to scale) of the instrument is given in Fig. 1.

2.1 CRDS Operation principals

The optical resonator consists of two mirrors (1 m radius of curvature) with nominal 0.999965 reflectivity at 405 nm (Advanced Thin Films), which are mounted 70 cm apart. The cavity volumes are defined by Teflon (FEP) coated Duran glass tubes with an inner diameter of 10 mm.

5   Under normal operating conditions each cavity samples 3.0 L (STD) min^{-1} (slm) of ambient air; additional purge flows (0.14 slm dry synthetic air) are introduced directly in front of each mirror to prevent surface degradation by atmospheric trace gases. The cavities are operated at pressures of 540 to 580 torr, resulting in residence time of ~1.2 s. 405 nm laser light (square-wave modulated at 1666 Hz and a 50% duty cycle) is provided by a laser diode (Laser Components), the emission of which is coupled into an optical fibre with a y-piece for splitting into both cavities. Temperature and current control of the laser diode

10 are achieved by a Thorlabs ITC 502 control unit. The laser emission spectrum is monitored continuously by coupling scattered light from one of the cavity mirrors into a 3648 pixel CCD-spectrograph (OMT, ~ 0.1 nm resolution).

The intensity of light exiting the cavity is measured with a photomultiplier (Hamamatsu Photonics), with ring-up and ring-down profiles recorded by a digital oscilloscope (PicoScope 3000). NO_2 mixing ratios are derived from the decay constant (k or k_0) describing the exponential decrease in light intensity after the laser has been switched off:

15 $$[NO_2] = \frac{l}{d} \cdot \frac{1}{\sigma c} (k - k_0), \tag{1}$$

where c is the speed of light, σ is the effective absorption cross-section of NO_2 over the emission spectrum of the laser (Vandaele et al., 2002) and k and k_0 are the decay constant with and without NO_2 present in the cavity, respectively. k_0 is thus defined by the mirror reflectivity and light scattering by the dry, synthetic air.

The ratio l / d accounts for the difference between the physical length of the cavity (l) and the effective optical path length (d)

20 in which NO_2 is present, and for dilution effects. d is shorter than l due to the purge flows of zero air in front of the mirrors and a value of $l / d = 0.98$ was determined by adding a constant flow of NO_2 and varying the purge-gas flow rate (Schuster et al., 2009; Thieser et al., 2016). k_0 is typically determined every five minutes (for one minute) by overflowing the inlets with zero air (CAP 180, Fuhr GmbH). PTFE filters (47 mm diameter, 2 µm pore size) prevent aerosol particles entering the cavities. Raw data sets (i.e. ring-down constants) undergo a few basic corrections before further analysis: 1) Interpolation of k_0 onto the

25 k time-grid. The first three data points after switching from sampling to zeroing are discarded, to ensure a stable zero signal. The remaining data points of each zero cycle are averaged. Finally, a linear interpolation between the averaged k_0 values is performed, allowing subtraction of k_0 for each individual data point. 2) Depending on conditions of flow, pressure and inlet set-up, changes in flow resistance between the zeroing and sampling periods result in slight changes in the cavity pressure. The resulting change in Rayleigh scattering of the 405 nm light owing to a pressure change of 6.5 Torr was found to be

30 equivalent to a change of ca. 300 pptv in the NO_2 mixing ratio, which is in accordance with earlier experiments using previous versions of this instrumental setup (Thieser et al., 2016). 3) A further correction is associated with the difference in the Rayleigh scattering coefficient between dry air (during zeroing) and humid air (whilst taking ambient measurements). This effect was

corrected using the H_2O scattering cross-sections reported by Thieser et al. (2016), leading e.g. to a correction of 116 pptv at 70% RH and 20 °C.

2.2 Detection of NO_x

In order to measure NO (which does not absorb at 405 nm), it is converted to NO_2 by reaction (R6) with an excess of ozone
5   (O_3) which was generated by passing zero air over a Hg Pen-Ray lamp emitting at 185 nm, which was housed inside a glass vessel at ca. 980 torr pressure. The gas-stream containing O_3 is split up equally by critical orifices and directed into two identical reaction-volumes made of 88 cm long PFA tubing (1/2 inch outer diameter, residence time 1.05 s). The concentration of O_3 (monitored by a commercial monitor, Model 202, 2B Technologies) was optimised in laboratory experiments in which the efficiency of conversion of NO to NO_2 was varied by variation of the flow of air over the Pen-Ray lamp. The maximum
10   concentration of NO_2 (and thus optimal conversion of NO to NO_2) was observed when the flow over the pen-ray lamp was between 60 and 80 sccm, corresponding to 19 ppmv O_3 in the reaction volumes. This result could be confirmed by numerical simulation (FACSIMILE) of the reactions involved in the formation and loss of NO_2 when NO reacts with O_3. According to the simulation, maximum conversion of NO to NO_2 during the 1.05 s residence time occurs between ca. 12 and 20 ppmv O_3. The conversion efficiency decreases at higher O_3 concentrations due to the formation of N_2O_5 and NO_3. The results from
15   experiments to determine the optimum parameters for O_3 generation are summarised in Fig. S1.

2.3 Thermal dissociation inlets: Detection of NO_y

The thermal dissociation inlets used to dissociate NO_y to NO_2 are made of quartz tubes housed in commercial furnaces (Carbolite, MTF 10/15/130). The oven temperature was regulated with a custom made electronic module, which enabled spatial separation between the heating elements and insulation and the control electronics. The distance between the heated
20   section of the quartz tubes and the point at which air was taken into the inlet was kept short in order to minimise losses of trace gases with a high affinity for surfaces, especially HNO_3 (Neuman et al., 1999). Experiments characterising the thermal conversion of various trace gases to NO_2 are described in Sect. 3.1. An electronic, 3-way valve under software control switches between the two heated inlets, one of which is equipped with a denuder. When sampling ambient air via the denuder we expect to remove all gas phase NO_y components and thus measure only particle borne nitrates (pNit). Experiments to characterise the
25   transmission of the denuder for particles and various trace gases are presented in Sect. 3.3.

2.4 Active carbon denuder

The active carbon denuder (DynamicAQS) has a honeycomb structure with 225 quadratic channels (1mm × 1 mm) of length 10 cm in a cylindrical form (diameter 3 cm) which is housed inside an aluminium casing with ½ inch connections (see Fig. 1). The geometric surface area of the denuder is ~ 45 cm^2. Assuming a specific surface area for activated carbon of 1000 m^2g^{-1}
30   (Atsuko et al., 1996), we calculate a BET surface area in the order of 10^8 cm^2.

2.5 Chemicals

A stock, liquid sample of PAN in n-tridecane (98+%, *Alfa Aesar*) was synthesized according to the procedures described by Gaffney et al. (1984) and Talukdar et al. (1995). Samples of lower concentration (as used in the experiments described below) were produced by diluting the original sample with additional n-tridecane. Acetone (> 99%), isopropyl nitrate (> 98.0%) and

5   (R)-(+)-limonene (97%) were obtained from *Sigma-Aldrich*. An ammonia permeation source (324 ng/min) was provided by *VICI Metronics*. Methanol (> 99.9%) was acquired from *Merck*, isoprene (98%, stabilised) from *Acros Organics* and ethanol from *Martin und Werner Mundo oHG*. Both nitric acid (65%) and β-pinene (pure) were obtained from *Roth*. The aqueous FEP dispersion (FEPD 121) was provided by *Chemours*.

3 Results and discussion

10   ### 3.1 Trace-gas thermograms

The fractional conversion of NO_z to NO_2 in the TD-inlets was investigated in a series of experiments in which constant flows of (separately) PAN, isopropyl nitrate and nitric acid were passed through the heated-inlet (bypassing the denuder) while the temperature was varied and NO_2 was monitored. Data were collected both during the heat-up and the cool-down periods of the oven. NO_x impurity levels were determined either via the simultaneous operation of the NO_x channel or via the NO_y channel

15   mixing ratio at room temperature, before and after heating the inlet.

3.1.1 PAN

A stream of 200 sccm synthetic air was used to elute a constant supply of gaseous PAN from its solution (held at a constant temperature of 0 °C in a glass vessel) into the CRDS inlet. The thermogram, a plot of the relative amount of NO_2 derived from PAN versus oven temperature, is presented in Fig. 2, the NO_2 mixing ratios are depicted in Fig. S2a). In this experiment the

20   maximum amount of NO_2 observed (at temperatures > 400 °C) was 2.2 ppbv. At temperatures < 100 °C, there was no measureable thermal decomposition of PAN to NO_2. Increasing the temperature from 100 °C to 300 °C results in a sharp increase in NO_2 which flattens off at temperature > 380 °C. We conclude that PAN is stoichiometrically converted to NO_2 at temperatures above 400 °C in our oven. The steepest part of the isotherm at ~200 °C, i.e. 50% conversion of PAN to NO_2, is therefore shifted by ca. 80 °C compared to those reported in the literature by Wild et al. (2014), Thieser et al. (2016) and

25   Sobanski et al. (2016). This is a consistent feature of our TD-ovens and is related to the short time available for thermal decomposition (see below).

3.1.2 Isopropyl nitrate

A 10 L stainless-steel canister containing 8.9 ppmv of isopropyl nitrate (iPN) at a pressure of 4 bar N_2 was prepared using a freshly vacuum-distilled liquid sample using standard manometric methods. In the freshly prepared canister NO_x impurities

were ~ 150 pptv. The thermogram obtained using iPN (Fig. 2 and Fig. S2b)) is noticeably broad, with NO_2 formed by thermal dissociation increasing slowly from 0.2 at 300 °C to 7.5 ppbv at 700 °C. Based on the mixing ratio of iPN in the canister and the dilution flows, this represents 90 ± 11% of the expected NO_2. The shaded area around the expected iPN mixing ratio in Fig. S2b) signifies the uncertainty of this value, based on propagation of the errors during the manometric and dilution

5 procedures (2% for flow rates, 5% for pressures measured with digital pressure gauges and 10% for the last dilution step using the analog pressure gauge of the canister).

Between 750 and 850 °C the thermal dissociation of iPN yields 7.8 ppbv NO_2. For iPN, the temperature at 50% conversion is 150 °C higher than those reported by Thieser et al. (2016) and Sobanski et al. (2016). Wild et al. (2014) employed a gaseous mixture of different alkyl nitrates and also observed a broad thermogram, with a sharp increase up to 80% conversion until

10 300 °C, followed by a slower increase until 800 °C. The alkyl nitrates thermogram from Wild et al. (2014) has been included into Fig. S2b) to illustrate this behaviour and to facilitate direct comparison.

3.1.3 HNO_3

A custom-made permeation source was used to provide a constant, known flow of HNO_3 to the TD-CRDS inlet. The permeation source consisted of a length (≈ 1m) of PFA tubing immersed in 66% HNO_3 solution held at 50 °C through which

15 100 sccm of dry, zero-air was passed. The concentration of HNO_3 and thus its permeation rate (1.62×10^{-4} sccm) was derived by measuring the optical extinction of HNO_3 at 185 nm using a literature absorption cross section (Dulitz et al., 2018). For a dilution flow of 7.6 slm, HNO_3 mixing ratios of 13.0 ppbv could be maintained, with ~ 1 ppbv NO_x as an interference. The HNO_3 thermogram (Fig. 2 and Fig. S2c)) indicates complete conversion of HNO_3 to NO_2 at temperatures above ≈ 800 °C. The amount of HNO_3 detected as NO_2 in the TD-CRDS in the plateau is 13.0 ppb, which is 85 ± 11% of that expected based on

20 the permeation- and dilution flows. Previous studies found complete conversion of HNO_3 to NO_2 at 600 °C (Wild et al., 2014) or 650 °C (Day et al., 2002; Womack et al., 2016).

The temperatures for 50% dissociation we measured for PAN, iPN and HNO_3 are higher than those reported in the literature (Day et al., 2002; Wild et al., 2014; Sobanski et al., 2016; Thieser et al., 2016; Womack et al., 2016), with shifts of 80 °C for PAN and 150 °C for iPN and HNO_3, respectively. This is likely to result from differences between the temperature sensed by

25 the thermocouple inside the heating element and the actual temperature of the gas stream, which, on average will be cooler. The requirement of higher temperatures in our oven is also a result of the rather short heated section (3 cm) in which the gas residence time is only a few ms. Based on the same kinetic rate constant parameters used by Day et al. (2002) for the dissociation reaction of PAN (Bridier et al., 1991), iPN (Barker et al., 1977) and HNO_3 (Glänzer and Troe, 1974), we calculated the theoretical 50% conversion temperature as a function of residence time inside the oven (see Fig. S2c)). For HNO_3, this

30 temperature increases by 40 °C from a 30 ms to a 10 ms residence time. In practise, we know neither the average temperature of the gas at the centre of the oven, nor can we characterise the axial and radial gradients in temperature in the quartz tubes, so that the thermograms serve only to determine the temperature needed to ensure complete conversion of each trace gas to NO_2.

These observations are broadly consistent with the observations of Womack et al. (2016) who find significant variations in degree of dissociation with sampling flow rate and residence time inside the heated area of the inlet. With the thermograms discussed above and considering the experimental uncertainties, however, we were able to verify quantitative PAN, iPN and

5   HNO$_3$ conversion to NO$_2$ in our TD-CRDS system at the chosen set temperature of 850 °C.

3.1.4 NH$_3$

As described previously (Wild et al., 2014; Womack et al., 2016) ammonia represents a potential interference in NO$_y$ measurements. In order to quantify this interference, we measured NO$_2$ formation in air containing 131 ppbv NH$_3$ delivered by a calibrated permeation source (VICI METRONICS, permeation rate 324 ng min^{-1} at 45 °C). The results are summarised

10   in Fig. 2. In NH$_3$ – air mixtures, we observe a small NO$_2$ signal, increasing at first slowly and then (from ≈ 700 °C) rapidly with temperature; the amount of NO$_2$ observed at 850 °C corresponds to a fractional conversion of NH$_3$ to NO$_2$ of 0.006 ± 0.002. This result is in broad agreement with Wild et al. (2014), who found a conversion efficiency of < 0.01 at 700 °C. In experiments with NH$_3$ in zero-air with relative humidities of 17%, 31% and 53% we were unable to observe conversion of NH$_3$ to NO$_2$, again consistent with humidity related suppression of NO$_2$ formation observed by Wild et al. (2014).

15   In additional experiments, we investigated the potential influence of ozone on the NH$_3$ to NO$_2$ conversion efficiency in zero-air containing O$_3$. The addition of O$_3$ results in a significant increase in NO$_2$ with a linear dependence on the O$_3$ mixing ratio (Fig. 3) with up to 11.4% conversion of NH$_3$ to NO$_2$ at 200 ppbv O$_3$. This was not reduced measurably by the addition of water vapour to the air / O$_3$ mixture. In further experiments we spiked air with the head-space of various organic liquids (acetone, methanol, ethanol, beta-pinene, limonene and isoprene). The gas-phase mixing ratios of the organic trace gases were unknown

20   but in each case the formation of NO$_2$ was suppressed or completely stopped. A more quantitative investigation was carried out using a known concentration (1 ppmv gas bottle) of isoprene. We found that addition of 30 ppbv isoprene to zero-air did not significantly reduce the NH$_3$-to-NO$_2$ conversion efficiency under dry conditions, but reduced it by a factor of two when the RH was increased to 50%.

A tentative chemical mechanism, based partially on Womack et al. (2016) to explain the formation of NO$_2$ from NH$_3$ and O$_3$

25   at high temperatures and the processes that suppress it is given in reactions (R11 to R15). In this scheme, the oxidation of NH$_3$ is initiated and propagated by O(^{3}P), formed from the thermal dissociation of O$_3$ (Peukert et al., 2013). This leads to formation of NO and HNO (R13a and R13b), both of which can be oxidised to NO$_2$ (R14 and R15). Forward and reverse rate coefficients for reaction (R11) indicate that O$_3$ is converted almost stoichiometrically to O(^{3}P) in the ≈ 10 ms reaction time in the heated inlet. The rate constants (at 1123 K) for the subsequent reactions involving O(^{3}P) are: k_{12} = 4.4 × 10^{-13} cm^3 molec^{-1} s^{-1} k_{13a} =

30   8.3 × 10^{-12} cm^3 molec^{-1} s^{-1} and k_{13b} = 7.5 × 10^{-11} cm^3 molec^{-1} s^{-1}) (Cohen and Westberg, 1991). Reaction (R12) converts 0.3% of the initial NH$_3$ molecules to NH$_2$ within 10 ms (at 100 ppbv O$_3$ and 1123 K).

$$O_3 + M \qquad \rightarrow O(^3P) + O_2 + M \qquad\qquad (R11)$$

$$O(^3P) + NH_3 \qquad \rightarrow NH_2 + OH \qquad\qquad (R12)$$

$$NH_2 + O(^3P) \qquad \rightarrow NO + H_2 \qquad\qquad (R13a)$$

$$\qquad\qquad\qquad \rightarrow HNO + H \qquad\qquad (R13b)$$

5 $\quad HNO + O(^3P) \,/\, OH \,/\, H \rightarrow NO + OH \,/\, H_2O \,/\, H_2 \qquad\qquad (R14)$

$$NO + O(^3P) + M \;\rightarrow NO_2 \;+ M \qquad\qquad (R15)$$

The experimental results obtained in zero-air indicate that reactions involving $O(^3P)$ from O_3 pyrolysis can result in the conversion of NH_3 to NO and NO_2. These results could however not be reproduced when adding NH_3 to ambient air sampled

10 from outside of the building. In this case, the addition of NH_3 (at 50-60 ppbv O_3) did not result in a measureable increase in NO_2, which was in accord with the observations of Womack et al. (2016). The scavenging of NH_2 radicals and O atoms by both volatile organic compounds and H_2O provides a likely explanation for this. Womack et al. (2016) also found that addition of 100 ppbv CO can reduce the conversion of NH_3 to NO_x.

In summary, our experiments indicate that the conversion of NH_3 to NO_2 is suppressed in ambient air samples, or in synthetic

15 air with added VOCs and water. The ambient air used in these experiments was from an urban and polluted environment (typical NO_x levels between 10 and 50 ppbv, see Sect. 4.2). As high levels of atmospheric NH_3 are associated with agricultural activity (Langford et al., 1992; Schlesinger and Hartley, 1992) and are often accompanied by high NO_x and VOC levels, the NH_3 interference under these conditions is most likely to be small compared to ambient NO_z levels. Long term measurements of NH_3 have additionally found a positive correlation between NH_3 concentrations and ambient temperature (Yamamoto et al.,

20 1988; Wang et al., 2015; Yao and Zhang, 2016), the latter promoting the presence of high levels of biogenic VOCs, such as isoprene (Tingey et al., 1979), which would also help to minimize the NH_3-related interference.

3.2 Bias caused by secondary reactions in the TD-ovens

Thermal dissociation techniques coupled to CRD-systems for measurement of organic nitrates suffer bias to different degrees owing to reactions of organic peroxy radicals with NO and NO_2 (Sobanski et al., 2016; Thieser et al., 2016). According to

25 previous studies (Day et al., 2002; Rosen et al., 2004; Thieser et al., 2016), in experiments using iPN at an oven temperature of 450 °C, an overestimation of ANs in the presence of NO is caused by reactions of the initially formed alkoxy radical, C_3H_7O, which results in the formation of both HO_2 and CH_3O_2 (R16-R21).

$$C_3H_7ONO_2 + M \rightarrow C_3H_7O + NO_2 + M \qquad\qquad (R16)$$

30 $\quad C_3H_7O + O_2 \rightarrow CH_3C(O)CH_3 + HO_2 \qquad\qquad (R17)$

$$C_3H_7O + M \rightarrow CH_3 + CH_3CHO + M \qquad\qquad (R18)$$

$$CH_3 + O_2 + M \rightarrow CH_3O_2 + M \qquad\qquad (R19)$$

$$CH_3O_2 + NO \rightarrow CH_3O + NO_2 \qquad\qquad (R20)$$

$$HO_2 + NO \rightarrow HO + NO_2 \qquad\qquad (R21)$$

$$CH_3C(O)O_2 + NO_2 + M \rightarrow CH_3C(O)O_2NO_2 + M \qquad\qquad (R22)$$

$$CH_3C(O)O_2 + M \rightarrow CH_3CO + O_2 + M \qquad\qquad (R23a)$$

5 $$CH_3C(O)O_2 \rightarrow CH_2C(O)OOH \qquad\qquad (R23b)$$

$$OH + NO_2 + M \rightarrow HNO_3 + M \qquad\qquad (R24)$$
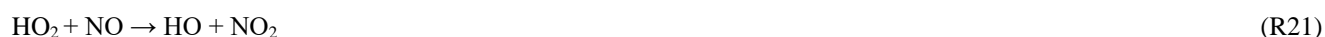
In order to investigate the potential bias in the measurement of ANs under the present experimental conditions, a set of experiments was conducted in which NO (up to 12 ppbv) was added to various amounts of iPN. The NO mixing ratio was

10 determined by modulating the addition of O_3. The results (Fig. 4a)), show that NO_2 derived from the thermal decomposition of iPN increases with the amount of NO added and results in overestimation (factor of ~1.6) at 12 ppbv NO, which is consistent with the observations by Thieser et al. (2016). This disappears when 19 ppmv ozone is added in front of the cavity so that NO_x rather than NO_2 is measured (blue data points). This is readily explained by the compensation of the additional NO_2 formed via reactions of NO with RO_2 by an equal loss in NO, which is only detected when introducing O_3. This is illustrated graphically

15 in Fig. S3.

We also explored the potential for bias caused by the recombination of $CH_3C(O)O_2$ and NO_2 when measuring PAN (reaction R22). Thieser et al. (2016) reported that PAN was underestimated by a factor 0.45 when adding 10 ppbv NO_2 to an air sample containing PAN at 200 °C. This behaviour was not apparent at 450 °C, which is related to the decomposition (reaction R23a) or isomerisation (reaction R23b) of $CH_3C(O)O_2$ at the higher temperature. The results of a similar experiment with our 850 °C

20 inlet are presented in Fig. 4b). In this plot, the measured NO_z relative to the input PAN is plotted versus the mixing ratio of added NO_2. For PAN concentrations from 1.5-2.2 ppbv no effect was observed for NO_2 concentrations of up to 10 ppbv. This is consistent with the reaction scheme presented by Thieser et al. (2016) at 450 °C.

A potential source of bias when measuring HNO_3 includes its reformation via the reaction of OH and NO_2 (reaction R24). Compared to the RO and RO_2 radicals formed in the thermal dissociation of PNs and ANs, OH exhibits a higher affinity for

25 surfaces and is likely to be efficiently removed at the oven wall. Day et al. (2002) estimated that wall losses are the dominant OH sink and that the resulting underestimation of HNO_3 would be < 2%, for NO_y levels < 5 ppbv. At our oven temperature, the diffusion coefficient for OH (D_{OH}) can be calculated according to Tang et al. (2014):

$$D_{OH}(1123 \text{ K}) = D_{OH}(296 \text{ K}) \cdot \frac{296^{-1.75}}{T} \,. \qquad\qquad (2)$$

Using an average of the literature values for D_{OH} at room temperature from Ivanov et al. (2007) (165 Torr cm^2 s^{-1}) and Bertram

30 et al. (2001) (192 Torr cm^2 s^{-1}), a value of $D_{OH}(1123 \text{ K}) = 1841$ Torr cm^2 s^{-1} was derived. The maximum rate constant for OH wall loss (assuming laminar flow) can subsequently be approximated according to Zasypkin et al. (1997):

$$k_{wall} = \frac{D_{OH} \cdot 3.66}{r^2 \cdot p}, \qquad\qquad (3)$$

With the radius of the oven quartz tube r (0.45 cm) and the pressure p (760 torr), the maximum value of k_{wall} is 44 s^{-1}. The first-order loss rate coefficient for reaction of OH with NO$_2$ is given by $k_{(OH+NO2)}$[NO$_2$], where $k_{(OH+NO2)}$ is the rate coefficient for reaction between OH and NO$_2$ at 1123 K (~ 5 x 10^{-14} cm^3 molec^{-1}s^{-1} (IUPAC, 2019) and [NO$_2$] = 6.5×10^{10} molecule cm^{-3} the concentration of 10 ppb NO$_2$ at the pressure and temperature of the oven. The first-order loss rate of OH via reaction with

5 NO$_2$ is then 3×10^{-3} s^{-1}. Clearly, the efficiency of uptake of OH to the wall would have to be very low in order to reduce the maximum value of 44 s^{-1} to values that are comparable to reaction with NO$_2$, which is very unlikely. We conclude that reformation of HNO$_3$ via reaction (R24) will not bias measurements of HNO$_3$ with the present set-up.

3.3 Denuder characterisation

The efficiency of removal of NO$_y$ trace gases and transmission of submicron particles was determined in a series of
10 experiments, which are described below:

3.3.1 Transmission of ammonium nitrate particles (10 – 414 nm)

In order to characterise the transmission of the denuder for particles of different diameter a constant flow of particles was generated by passing 3.3 slm of nitrogen through an atomizer (TSI 3076) containing an aqueous solution of ammonium nitrate. The flow rate (3.3 slm) was matched to the typical sampling flow through the denuder. 0.28 slm of the flow was sampled into
15 an SMPS/CPC system (TSI 3080 and TSI 3025A) to measure the number density and size distribution (10 – 414 nm) of the ammonium nitrate particles. The flow was delivered either directly to the SMPS/CPC via straight metal tubing (length 27 cm, inner diameter 0.9 cm), for which we assume 100 % particle transmission, or via the denuder. The ratio of the particle numbers in each size bin thus represents the size-dependent denuder transmission. As shown in Fig. 5, the transmission of the denuder is > 80 % for particles between 30 and 400 nm diameter. As expected, some diffusive loss is observed for particles < 20 nm
20 diameter and loss due to impaction / settling is observed for particles > 300 nm. The particle transmission T as a function of particle diameter d can represented by the following empirical expression:

$$T(\%) = \frac{d(nm)-5.79}{0.035+0.010 \cdot (d-5.79)+1.78 \cdot 10^{-6} \cdot (d-5.79)^2}. \tag{4}$$

The particle transmission through the denuder channels was also calculated using the *Particle Loss Calculator (PCL)*
25 developed by von der Weiden et al. (2009). The results of this calculation are also plotted in Fig. 5. The observed loss of particles smaller than 40 nm are not replicated by the *PCL*, which was developed for cylindrical piping and not the square honeycomb shape of the denuder and also does not take into account losses due to impact at the finite surface area which the gas/particle flow is exposed to at the entrance to the honeycomb.

3.3.2 Efficiency of removal of NO$_y$ trace gases.

The efficiency of removal of trace gases in the denuder under typical flow conditions (3.3 slm) was investigated for NO, NO$_2$, PAN, iPN and HNO$_3$ as representative NO$_y$ species. The efficiency of removal of each trace gas (generally present at 5-40 ppbv) was determined by measuring its relative concentration when flowing through the denuder (pNit-channel) and when

5   bypassing the denuder (NO$_y$ channel). The results (Fig. 6) indicate that, in dry air, all of these trace gases were removed with an efficiency of close to 100 %. However, when the main dilution flow was humidified significant, RH-dependent breakthrough of NO was observed, with only 60 % stripped from the gas-phase at RH close to 100 %. In contrast, humidification had only a marginal effect on the scrubbing efficiency for NO$_2$, iPN and HNO$_3$ for which an efficiency of $\geq$ 95 % was observed.

10   In further experiments, we examined the potential for re-release of NO$_y$ that had previously been stored in the activated carbon substrate of the denuder. In these experiments, in which either NO$_x$ or NO$_y$ was continuously monitored, the denuder was exposed to a flow of 9.5 ppm iPN in dry nitrogen for 90 minutes during which 2.30 x 10^{17} molecules of iPN were stripped from the gas phase and deposited onto the denuder. This exposure is equivalent to a month-long exposure to 20 ppb of iPN. The air passing through the denuder was subsequently humidified to RH = 65 %. The results (Fig. 7a)) indicate a high initial

15   (11:40 – 11:50) rate of release of NO$_x$ under humid conditions (resulting in a maximum mixing ratio of 2 ppbv at 11:45). At 11:50, humidification of the air was stopped and the rate of release of NO$_x$ dropped gradually towards zero. During a second period, in which the air was again humidified (from 11:50 on), NO$_x$ was released from the denuder, albeit at a lower rate than during the first humidification. From 12:25 onwards, the oven behind the denuder was heated to 850 °C so that NO$_y$ was added. No significant increase in NO$_2$ was observed indicating that the trace-gas(es) species released from the denuder surface upon

20   humidification are predominantly NO$_x$. During this experiment, 2.55 x 10^{15} NO$_x$ molecules desorbed from the denuder, indicating that the major fraction of iPN molecules remained stored on the denuder surface upon humidification.

Similar denuder exposure experiments were performed with HNO$_3$ and NO$_2$. For HNO$_3$, no evidence for desorption of NO$_x$ or NO$_y$ during exposure to humidified air was observed, whereas NO$_2$ exhibited a similar behaviour to iPN (Fig. 7b)). After loading the denuder with 5 sccm from a 0.831 ppm NO$_2$ gas bottle for 4.8 days (a total of 7.60 x 10^{17} molecules deposited),

25   the effect of passing humidified air through the denuder was to release NO$_x$, which was observed at concentrations up to $\approx$ 39 ppbv. While the relative humidity was kept constant at close to 100 %, the NO$_x$ released decreased over time so that after 30 minutes, 3.2 ppbv NO$_x$ could still be detected. By switching the O$_3$ source off (at $\approx$ 10:45) the NO$_2$ measured went to $\approx$ zero indicating that predominantly NO was released (and not NO$_2$). Integrating these results over time yielded a value of 1.63 x 10^{16} molecules desorbed NO from the denuder surface in humid air.

30   Clearly, adsorption of water molecules onto the denuder surface can initiate / catalyse chemical transformation at the surface than convert stored NO$_z$ into forms than can desorb and be detected as NO$_x$. To further our understanding of underlying processes that occur upon humidification, a series of experiments were conducted to examine the adsorption of water on the denuder. In these experiments the denuder was first dried by exposing it to dry air for several hours until the relative humidity

of the air exiting the denuder was close to zero. Subsequently, humidified air was passed through the denuder and the RH of air exiting it was continuously monitored. The results of an experiment in which the air was humidified to 68 % are shown in Fig. 8a). After 77 minutes of exposure to this humidity, the RH of the air exiting the denuder acquired a maximum value of 64%. After switching back to dry synthetic air (at 09:37 UTC), ~60 minutes passed before the RH dropped to values close to zero. In this period, the RH did not decrease monotonically, the rate of change of relative humidity exiting the denuder revealing a number of discreet steps. Figure 8b) plots the derivatives (dRH/dt) of the drying phases of a series of experiments in which the initial RH was varied between 47 and 75 %. A similar pattern emerges for each experiment with the greatest desorption rates occurring at the beginning of the drying phase followed by a minimum in the desorption rate and a second maximum (at $\approx$ 15 % relative humidity). This behaviour is a clear indication that H_2O is bound to more than one chemically or physically distinct surface sites on the activated-activated carbon.

By measuring the change in RH of the air flowing into and out of the denuder we can derive an equilibrium adsorption isotherm for H_2O at the active carbon surface. An example is given in Fig. 9 where it is also compared to a literature isotherm for adsorption of water vapour on activated carbon fibre (Kim et al., 2008). The data of Kim et al. (2008) have been scaled, by matching the number of adsorbed water molecules at 65.9 % RH to our observed value at 67.2 % RH. The exposure of carbonaceous surfaces to inert gases at high temperatures (2000 °C) reduces the capacity for water uptake, whereas functionalising the carbon surface with oxygen containing groups (e.g. from HNO_3) enhances the water adsorption capacity (Dubinin et al., 1982; Barton and Koresh, 1983; Liu et al., 2017). In our experiments, the uptake of gas-phase NO_y is thus expected to generate oxygenated sites on our denuder surface, which in turn will influence water uptake and thus further trace-gas accommodation.

The chemistry leading to the formation of gas-phase NO_x from NO_y trace-gases adsorbed at the denuder surface under humid conditions cannot be elucidated in detail with our experimental setup. However, a strong humidity dependence in the heterogeneous generation of HONO and NO from NO_2 adsorbed on soot particles has been reported (Kalberer et al., 1999; Kleffmann et al., 1999). Formation of HONO from NO_x has also been observed on wet aerosol and ground surfaces in field studies (Lammel and Perner, 1988; Notholt et al., 1992). Previous investigations report the adsorption of NO_2 on activated carbon at ambient or close to ambient temperatures (30-50 °C), followed by its reduction to NO, with the simultaneous oxidation of the carbon surface (Shirahama et al., 2002; Zhang et al., 2008; Gao et al., 2011). These results are consistent with our observation of e.g. conversion of NO_2 to NO at the denuder surface under humid conditions. In our experiments, we observed that NO_2 was converted to NO (rather than HONO) at the denuder surface. It is possible that the initial step is formation of HONO (e.g. by the surface catalysed hydrolysis of NO_2 or iPN) which undergoes further reduction on the surface to NO. Release of HONO and NO has also been observed from soil, after the nitrification of NH_3/NH_4^+ or the reduction of NO_3^- (Su et al., 2011; Pilegaard, 2013; Meusel et al., 2018). Oswald et al. (2013) found comparable HONO and NO emission fluxes from non-acidic soils, providing another example of heterogeneous formation of HONO from other atmospheric nitrogen species, followed by the gas phase release of NO.

We conclude that the use of this denuder type (and assumption of complete removal of gaseous NO_y) may potentially result in a positive bias in measurements of particle nitrate owing to variable breakthrough and release of NO_x (dependent on the historical exposure of the denuder and relative humidity). Our findings may be applicable (at least in a qualitative sense) to similar denuders using activated carbon surfaces, and careful characterisation of the capacity to adsorb, breakthrough and release of NO_y components should be carried out prior to use in the field.

Reliable surface re-activation techniques for similar denuders would be useful to ensure continuous, efficient scrubbing of NO_y and NO_x and circumnavigate the potential overestimation of pNit. In this regard, attempts to "reactivate" the denuder by cleaning with distilled water, drying at 50 °C and exposure to ca. 300 ppbv O_3 for one hour did not result in an improvement of the direct NO-breakthrough or in the background pNit signal upon humidification. Surface sensitive, spectroscopic investigation of the water-induced transformation of organic and inorganic NO_y to NO_x (and its subsequent release to the gas-phase) on denuder surfaces would be useful in resolving these issues.

4 Application of the instrument in field experiments

4.1 NO_x intercomparison and pNit measurements during the AQABA campaign

The first deployment of the instrument was during the AQABA (*A*ir *Q*uality and climate change in the *A*rabian *Ba*sin) ship campaign in summer 2017. From the 31st of July to the 2nd of September, this campaign followed a route from southern France via the Mediterranean Sea, the Suez Channel, the Red Sea, the Arabian Sea and the Arabian Gulf to Kuwait and back. The instrument was placed in a shipping container in front of the exploration ship *Kommander Iona*, with the inlet ovens located in an aluminium box on the roof of the container. The (unheated) tips of quartz inlet tubes protruded about 15 cm from the side of the aluminium box.

Here we report only the NO_x and pNit measurements, an analysis of the NO_z data will be reported in a separate publication.

During AQABA, NO_x levels ranged from a few pptv (maritime background) up to several tens of ppbv in heavily polluted air masses in shipping lanes or in harbours. In Fig. 10a) we compare NO_x measured with the TD-CRDS with the results of an chemiluminescence detector (CLD 790 SR, ECO Physics, Tadic et al. (2019)), which measured NO and NO_2. The data points represent 1 minute averages for the entire campaign, excluding air-masses which were contaminated by the ships exhaust. Additionally, periods with very high NO_x variability were not included, a data point being discarded whenever the differences in mean values exceeded 2 ppbv for consecutive data points.

A bivariate fit to the datasets (York, 1966), which incorporates total uncertainties for both instruments (CLD: 8.6%; TD-CRDS: 11% + 20 pptv*RH/100) resulted in a slope of 0.996 ± 0.003 and an intercept of -1.3 pptv, which indicates very good agreement, which is well within the combined uncertainty of the instruments. The good agreement serves to underline the general applicability of the TD-CRDS in NO_x measurements even under difficult conditions (e.g. a non-static platform).

Figure 10b) shows a ca. 10 hours time frame with pNit measurements from the denuder channel of the TD-CRDS. Unfortunately, the TD-oven of the denuder channel broke down very early in the campaign and was not operational afterwards. The data from the pNit channel are presented together with the NO_x and NO_y measurements along with particulate nitrate mass concentrations measured by an aerosol mass spectrometer (Aerodyne HR-ToF-AMS; DeCarlo et al. (2006), Brooks et al.

5   (2020)). The night-to-day transition is indicated via NO_2 photolysis rates J_{NO2} derived from a spectral radiometer (Metcon GmbH), the relative humidity was > 80 % throughout the period shown. During the two periods when, apart from some short spikes, NO_x was very low (21:10-23:45 UTC and 02:20-03:40 UTC), TD-CRDS data indicate the presence of 300-400 pptv of pNit, which would then constitute ~80% of NO_y. Such mixing ratios of particulate nitrate are not commensurate with those measured by the AMS, which, on average, are a factor 6-8 lower. As the AMS does not detect particles larger than ~1 μm

10   diameter with high efficiency, this could indicate that a significant fraction of the particulate nitrate is associated with coarse mode aerosol. In the lower panel of Fig. 10b) we plot coarse mode aerosol mass concentration determined from measurements of an optical particle counter (OPC) that measures particles between 0.2 and 20 μm. In the two low NO_x periods outlined above, the OPC-derived aerosol mass concentrations were between 3 and 5 μg m^{-3}. If 10 % of this coarse mode aerosol mass concentration were nitrate, which is a typical value in the Mediterranean (Koulouri et al., 2008; Calzolai et al., 2015; Malaguti

15   et al., 2015), this would account for 100-200 pptv of the pNit observed by the TD-CRDS and not by the AMS. However, the time profile of pNit measured by the TD-CRDS is not consistent with those of either the OPC or the AMS, but rather resembles the NO_x mixing ratios. This strongly suggests that the large difference between pNit reported by the TD-CRDS and the AMS does not results from the inability of the AMS to detect supermicron particulate nitrate, but from denuder artefacts similar to those seen in the laboratory experiments described in Sect. 3.3.2. This short case-study serves to highlight the potential positive

20   bias in denuder based, TD-CRDS measurements of pNit under humid field conditions.

4.2 Ambient NO_x and NO_y measurements in an urban environment (Mainz, Germany)

NO_x and NO_y mixing ratios were obtained in air sampled outside the Max-Planck-Institute for Chemistry (MPIC). The MPIC (49°59'27.5"N 8°13'44.4"E) is located on the outskirts of Mainz but within 200 m of two busy 2- and 4-lane roads and within 500 m of additional university buildings as well as commercial and residential areas. The city of Mainz (217k inhabitants) is

25   located in the densely populated *Rhine-Main-Area* together with the cities of Frankfurt (753k) and Wiesbaden (278k) and the air is strongly influenced by local pollution. The sampling location was on the top floor of a three story building (ca. 12 m above ground level). Air was sub-sampled to the inlets of the instrument from a ~1 m long 0.5 inch outer diameter PFA tube which was connected to a membrane pump / flow controller to generate a 20 slm bypass flow.

Figure 11a) summarises the 8-days of measurement (data coverage 82 %) as a time series for NO_x, NO_y, NO_z, (10 min averages)

30   wind speed (1 hour averages) and the NO_z/NO_y ratio. The NO_x and NO_y mixing ratios were highly variable throughout this period, with NO_x mixing ratios between 0.7 and 148.3 ppbv (mean and median values of 22.1 and 6.9 ppbv, respectively). Traffic-related morning rush-hour peaks in NO_x were observed on all weekdays (14th, 16th, 17th and 20th) between 5:00 and 10:00 UTC. The morning NO_x peak is reduced or absent on the weekends (18th and 19th). NO_x levels stayed above 50 ppbv for

nearly a full day from 18:00 UTC on the 16th of January until 18:00 UTC on the 17th of January, which coincides with constantly low wind speeds and sampling of air masses that were predominantly local, and thus highly polluted. NO_z mixing ratios were usually between 0.5 and 2.5 ppbv (minimum < LOD, maximum 3.1 ppbv, mean 1.0 ppbv and median 0.9 ppbv), with NO_z / NO_y ratios below 0.5. These values indicate that the air masses have been impacted by recent (local) NO_x emissions.

5 The NO_z/NO_y ratio can be used as indicator for the degree of chemical processing of an air mass. In Fig. 11b) a median diel profile (including all measurement days) for the NO_z/NO_y ratio from the ambient measurement is shown. The diel profile displays two distinct minima in NO_z / NO_y during the morning and evening rush hour, where NO_z only makes up 5-10 % of the total NO_y (which is dominated by freshly emitted NO_x). This fraction increases up to 15 % during midday and up to 25 % during nighttime during which emissions of NO_x are reduced. These measurements serve to illustrate the applicability of our

10 TD-CRDS over a wide range of NO_x and NO_y concentrations under realistic field conditions and in the investigation of processes that transform NO_x into its gas- and particle-phase reservoirs.

5 Conclusions

We report on the development, characterisation and first deployment of a TD-CRDS instrument for the measurement of NO_x, NO_y, NO_z and pNit. We show that the NO_z species PAN, iPN and HNO_3 are quantitatively converted to NO_2. The potential for

15 NH_3 to bias NO_y measurements was assessed and found to be insignificant in ambient air or synthetic air containing VOCs and water. The conversion to NO_2 (by reaction with O_3) of atmospheric NO, and also NO formed in the heated inlet circumvents bias resulting from O_3 pyrolysis (leading to an NO_2 overestimation) and secondary processes, initiated by the thermal dissociation of organic nitrates. For our activated carbon denuder, we observed > 90 % transmission for ammonium nitrate particles with diameters between 40 and 400 nm. Under humid conditions, however, the denuder exhibited a direct

20 breakthrough of NO and the re-release of previously stored iPN and NO_2 in form of NO, indicating a potential bias of pNit measurements using this technique. The performance of the instrument under field conditions was demonstrated by measurements in Mainz, Germany and during the AQABA ship campaign. NO_x measurements with the new instrument were in good agreement with those from an established, independent CLD-based instrument.

Author contributions

25 NF developed the TD-CRDS, performed all laboratory and campaign measurements, evaluated the data sets and wrote the manuscript. IT and HF provided the AQABA CLD NO_x measurements. JS designed the heated inlet system and performed actinic flux measurements on AQABA. JB, ED and FD provided AMS and OPC measurements from AQABA. JL and JNC designed and supervised the study and the campaigns. JNC, JL and FD contributed to the manuscript.

Competing Interests

The authors declare that they have no conflict of interest.

Acknowledgements

We thank Ezra Wood for providing us with the activated-carbon denuder and Chemours for the provision of the FEP sample
5 (FEPD 121) used to coat the cavity walls. This work was supported by the Max Planck Graduate Center with the Johannes
Gutenberg-Universität Mainz (MPGC).

References

Atsuko, N., Kazuya, S., Toshiaki, E., Kei-ichi, K., Morinobu, E., and Norifumi, S.: Electronic and Magnetic Properties of Activated Carbon
Fibers, Bull. Chem. Soc. Jpn., 69, 333-339, 10.1246/bcsj.69.333, 1996.
10
Barker, J. R., Benson, S. W., Mendenhall, G. D., and Goldern, D. M.: Measurements of rate constants of importance in smog, Rep. PB-
274530, Natl. Tech. Inf. Serv., Springfield, Va., 1977.

Barton, S. S., and Koresh, J. E.: Adsorption Interaction of Water with Microporous Adsorbents .1. Water-Vapor Adsorption on Activated
15 Carbon Cloth, J Chem Soc Farad T 1, 79, 1147-1155, DOI 10.1039/f19837901147, 1983.

Bertram, A. K., Ivanov, A. V., Hunter, M., Molina, L. T., and Molina, M. J.: The reaction probability of OH on organic surfaces of
tropospheric interest, J. Phys. Chem. A, 105, 9415-9421, 2001.

20 Beygi, Z. H., Fischer, H., Harder, H. D., Martinez, M., Sander, R., Williams, J., Brookes, D. M., Monks, P. S., and Lelieveld, J.: Oxidation
photochemistry in the Southern Atlantic boundary layer: unexpected deviations of photochemical steady state, Atmos. Chem. Phys., 11,
8497-8513, 10.5194/acp-11-8497-2011, 2011.

Bridier, I., Caralp, F., Loirat, H., Lesclaux, R., Veyret, B., Becker, K. H., Reimer, A., and Zabel, F.: Kinetic and Theoretical-studies of the
25 Reactions $CH_3C(O)O_2 + NO_2 + M <-> CH_3C(O)NO_2 + M$ between 248 K and 393 K and Between 30-torr and 760-torr, J. Phys. Chem., 95,
3594-3600, 1991.

Brooks, J., Darbyshire, E., Drewnick, F., Alfarra, R., Struckmeier, C., Fachinger, F., Borrmann, S., Allen, G., and Coe, H.: Characterisation
of accumulation mode aerosol across the Middle East and Mediterranean during a ship campaign in the summer of 2017, in preperation,
30 2020.

Calzolai, G., Nava, S., Lucarelli, F., Chiari, M., Giannoni, M., Becagli, S., Traversi, R., Marconi, M., Frosini, D., Severi, M., Udisti, R., di
Sarra, A., Pace, G., Meloni, D., Bommarito, C., Monteleone, F., Anello, F., and Sferlazzo, D. M.: Characterization of PM10 sources in the
central Mediterranean, Atmos Chem Phys, 15, 13939-13955, 10.5194/acp-15-13939-2015, 2015.
35
Cohen, N., and Westberg, K. R.: Chemical Kinetic Data Sheets for High-Temperature Reactions .2., J. Phys. Chem. Ref. Data, 20, 1211-
1311, Doi 10.1063/1.555901, 1991.

Day, D. A., Wooldridge, P. J., Dillon, M. B., Thornton, J. A., and Cohen, R. C.: A thermal dissociation laser-induced fluorescence instrument
40 for in situ detection of NO_2, peroxy nitrates, alkyl nitrates, and HNO_3, J. Geophys. Res. -Atmos., 107, doi:10.1029/2001jd000779, 2002.

Day, D. A., Dillon, M. B., Wooldridge, P. J., Thornton, J. A., Rosen, R. S., Wood, E. C., and Cohen, R. C.: On alkyl nitrates, O_3, and the
"missing NOy", J. Geophys. Res. -Atmos., 108, 4501, doi:10.1029/2003jd003685, 2003.

DeCarlo, P. F., Kimmel, J. R., Trimborn, A., Northway, M. J., Jayne, J. T., Aiken, A. C., Gonin, M., Fuhrer, K., Horvath, T., Docherty, K. S., Worsnop, D. R., and Jimenez, J. L.: Field-deployable, high-resolution, time-of-flight aerosol mass spectrometer, Anal. Chem., 78, 8281-8289, 10.1021/ac061249n, 2006.

5   Dubinin, M. M., Andreeva, G. A., Vartapetyan, R. S., Vnukov, S. P., Nikolaev, K. M., Polyakov, N. S., Seregina, N. I., and Fedoseev, D. V.: Adsorption of Water and the Micropore Structures of Carbon Adsorbents .5. Pore Structure Parameters of Thermally Treated Carbon Adsorbents and the Adsorption of Water-Vapor on These Materials, B Acad Sci Ussr Ch+, 31, 2133-2137, Doi 10.1007/Bf00958379, 1982.

Dulitz, K., Amedro, D., Dillon, T. J., Pozzer, A., and Crowley, J. N.: Temperature-(208-318 K) and pressure-(18-696 Torr) dependent rate
10   coefficients for the reaction between OH and HNO₃, Atmos. Chem. Phys., 18, 2381-2394, 2018.

Fahey, D. W., Eubank, C. S., Hubler, G., and Fehsenfeld, F. C.: Evaluation of a Catalytic Reduction Technique for the Measurement of Total Reactive Odd-Nitrogen Noy in the Atmosphere, J Atmos Chem, 3, 435-468, Doi 10.1007/Bf00053871, 1985.

15   Finlayson-Pitts, B. J., Ezell, M. J., and Pitts, J. N. J.: Formation of chemically active chlorine compounds by reactions of atmospheric NaCl particles with gaseous N₂O₅ and ClONO₂, Nature, 337, 241-244, 10.1038/337241a0, 1989.

Fry, J. L., Draper, D. C., Zarzana, K. J., Campuzano-Jost, P., Day, D. A., Jimenez, J. L., Brown, S. S., Cohen, R. C., Kaser, L., Hansel, A., Cappellin, L., Karl, T., Roux, A. H., Turnipseed, A., Cantrell, C., Lefer, B. L., and Grossberg, N.: Observations of gas- and aerosol-phase
20   organic nitrates at BEACHON-RoMBAS 2011, Atmos. Chem. Phys., 13, 8585-8605, 10.5194/acp-13-8585-2013, 2013.

Fuchs, H., Ball, S. M., Bohn, B., Brauers, T., Cohen, R. C., Dorn, H. P., Dube, W. P., Fry, J. L., Haseler, R., Heitmann, U., Jones, R. L., Kleffmann, J., Mentel, T. F., Musgen, P., Rohrer, F., Rollins, A. W., Ruth, A. A., Kiendler-Scharr, A., Schlosser, E., Shillings, A. J. L., Tillmann, R., Varma, R. M., Venables, D. S., Tapia, G. V., Wahner, A., Wegener, R., Wooldridge, P. J., and Brown, S. S.: Intercomparison
25   of measurements of NO₂ concentrations in the atmosphere simulation chamber SAPHIR during the NO₃-Comp campaign, Atmos. Meas. Tech., 3, 21-37, 2010.

Gaffney, J. S., Fajer, R., and Senum, G. I.: An Improved Procedure for High-Purity Gaseous Peroxyacyl Nitrate Production - Use of Heavy Lipid Solvents, Atmos Environ, 18, 215-218, Doi 10.1016/0004-6981(84)90245-2, 1984.

Gao, X. A., Liu, S. J., Zhang, Y., Luo, Z. Y., Ni, M. J., and Cen, K. F.: Adsorption and reduction of NO2 over activated carbon at low temperature, Fuel Process Technol, 92, 139-146, 10.1016/j.fuproc.2010.09.017, 2011.

Glänzer, K., and Troe, J.: Thermal Decomposition of Nitrocompounds in Shock Waves. IV: Decomposition of Nitric Acid, Berichte der
35   Bunsengesellschaft für physikalische Chemie, 78, 71-76, 10.1002/bbpc.19740780112, 1974.

Huang, W., Saathoff, H., Shen, X. L., Ramisetty, R., Leisner, T., and Mohr, C.: Chemical Characterization of Highly Functionalized Organonitrates Contributing to Night-Time Organic Aerosol Mass Loadings and Particle Growth, Environmental Science & Technology, 53, 1165-1174, 10.1021/acs.est.8b05826, 2019.
40
IUPAC: Task Group on Atmospheric Chemical Kinetic Data Evaluation, (Ammann, M., Cox, R.A., Crowley, J.N., Herrmann, H., Jenkin, M.E., McNeill, V.F., Mellouki, A., Rossi, M. J., Troe, J. and Wallington, T. J.) http://iupac.pole-ether.fr/index.html., 2019.

Ivanov, A. V., Trakhtenberg, S., Bertram, A. K., Gershenzon, Y. M., and Molina, M. J.: OH, HO2, and ozone gaseous diffusion coefficients,
45   J. Phys. Chem. A, 111, 1632-1637, 2007.

Javed, U., Kubistin, D., Martinez, M., Pollmann, J., Rudolf, M., Parchatka, U., Reiffs, A., Thieser, J., Schuster, G., Horbanski, M., Pöhler, D., Crowley, J. N., Fischer, H., Lelieveld, J., and Harder, H.: Laser-induced fluorescence-based detection of atmospheric nitrogen dioxide and comparison of different techniques during the PARADE 2011 field campaign, Atmos. Meas. Tech., 12, 1461-1481, 10.5194/amt-12-
50   1461-2019, 2019.

Kalberer, M., Ammann, M., Arens, F., Gaggeler, H. W., and Baltensperger, U.: Heterogeneous formation of nitrous acid (HONO) on soot aerosol particles, J. Geophys. Res. -Atmos., 104, 13825-13832, 1999.

55   Kim, P., Zheng, Y. J., and Agnihotri, S.: Adsorption equilibrium and kinetics of water vapor in carbon nanotubes and its comparison with activated carbon, Ind Eng Chem Res, 47, 3170-3178, 10.1021/ie0713240, 2008.

Kleffmann, J., Becker, K. H., Lackhoff, M., and Wiesen, P.: Heterogeneous conversion of NO2 on carbonaceous surfaces, Phys. Chem. Chem. Phys., 1, 5443-5450, DOI 10.1039/a905545b, 1999.

5 Koulouri, E., Saarikoski, S., Theodosi, C., Markaki, Z., Gerasopoulos, E., Kouvarakis, G., Makela, T., Hillamo, R., and Mihalopoulos, N.: Chemical composition and sources of fine and coarse aerosol particles in the Eastern Mediterranean, Atmos Environ, 42, 6542-6550, 10.1016/j.atmosenv.2008.04.010, 2008.

Lammel, G., and Perner, D.: The Atmospheric Aerosol as a Source of Nitrous-Acid in the Polluted Atmosphere, J. Aerosol Sci., 19, 1199-
10 1202, Doi 10.1016/0021-8502(88)90135-8, 1988.

Langford, A. O., Fehsenfeld, F. C., Zachariassen, J., and Schimel, D. S.: Gaseous Ammonia Fluxes and Background Concentrations in Terrestrial Ecosystems of the United States, Glob. Biogeochem. Cycles, 6, 459-483, 10.1029/92gb02123, 1992.

15 Lee, B. H., Mohr, C., Lopez-Hilfiker, F. D., Lutz, A., Hallquist, M., Lee, L., Romer, P., Cohen, R. C., Iyer, S., Kurten, T., Hu, W. W., Day, D. A., Campuzano-Jost, P., Jimenez, J. L., Xu, L., Ng, N. L., Guo, H. Y., Weber, R. J., Wild, R. J., Brown, S. S., Koss, A., de Gouw, J., Olson, K., Goldstein, A. H., Seco, R., Kim, S., McAvey, K., Shepson, P. B., Starn, T., Baumann, K., Edgerton, E. S., Liu, J. M., Shilling, J. E., Miller, D. O., Brune, W., Schobesberger, S., D'Ambro, E. L., and Thornton, J. A.: Highly functionalized organic nitrates in the southeast United States: Contribution to secondary organic aerosol and reactive nitrogen budgets, Proc. Natl. Acad. Sci. U. S. A., 113, 1516-1521,
20 10.1073/pnas.1508108113, 2016.

Leser, H., Honninger, G., and Platt, U.: MAX-DOAS measurements of BrO and NO2 in the marine boundary layer, Geophys Res Lett, 30, Artn 1537
10.1029/2002gl015811, 2003.
25
Lightfoot, P. D., Cox, R. A., Crowley, J. N., Destriau, M., Hayman, G. D., Jenkin, M. E., Moortgat, G. K., and Zabel, F.: Organic peroxy radicals - kinetics, spectroscopy and tropospheric chemistry, Atmos. Environ., Part A, 26, 1805-1961, 1992.

Liu, L. M., Tan, S. L., Horikawa, T., Do, D. D., Nicholson, D., and Liu, J. J.: Water adsorption on carbon - A review, Adv Colloid Interfac,
30 250, 64-78, 10.1016/j.cis.2017.10.002, 2017.

Logan, J. A.: Nitrogen-Oxides in the Troposphere - Global and Regional Budgets, J Geophys Res-Oceans, 88, 785-807, DOI 10.1029/JC088iC15p10785, 1983.

35 Malaguti, A., Mircea, M., La Torretta, T. M. G., Telloli, C., Petralia, E., Stracquadanio, M., and Berico, M.: Chemical Composition of Fine and Coarse Aerosol Particles in the Central Mediterranean Area during Dust and Non-Dust Conditions, Aerosol Air Qual Res, 15, 410-425, 10.4209/aaqr.2014.08.0172, 2015.

Merten, A., Tschritter, J., and Platt, U.: Design of differential optical absorption spectroscopy long-path telescopes based on fiber optics,
40 Appl. Opt., 50, 738-754, 2011.

Meusel, H., Tamm, A., Kuhn, U., Wu, D. M., Leifke, A. L., Fiedler, S., Ruckteschler, N., Yordanova, P., Lang-Yona, N., Pohlker, M., Lelieveld, J., Hoffmann, T., Poschl, U., Su, H., Weber, B., and Cheng, Y. F.: Emission of nitrous acid from soil and biological soil crusts represents an important source of HONO in the remote atmosphere in Cyprus, Atmos Chem Phys, 18, 799-813, 10.5194/acp-18-799-2018,
45 2018.

Murphy, J. G., Day, A., Cleary, P. A., Wooldridge, P. J., and Cohen, R. C.: Observations of the diurnal and seasonal trends in nitrogen oxides in the western Sierra Nevada, Atmos. Chem. Phys., 6, 5321-5338, 2006.

50 Neuman, J. A., Huey, L. G., Ryerson, T. B., and Fahey, D. W.: Study of inlet materials for sampling atmospheric nitric acid, Env. Sci. Tech., 33, 1133-1136, 1999.

Ng, N. L., Brown, S. S., Archibald, A. T., Atlas, E., Cohen, R. C., Crowley, J. N., Day, D. A., Donahue, N. M., Fry, J. L., Fuchs, H., Griffin, R. J., Guzman, M. I., Herrmann, H., Hodzic, A., Iinuma, Y., Jimenez, J. L., Kiendler-Scharr, A., Lee, B. H., Luecken, D. J., Mao, J., McLaren,
55 R., Mutzel, A., Osthoff, H. D., Ouyang, B., Picquet-Varrault, B., Platt, U., Pye, H. O. T., Rudich, Y., Schwantes, R. H., Shiraiwa, M., Stutz,

J., Thornton, J. A., Tilgner, A., Williams, B. J., and Zaveri, R. A.: Nitrate radicals and biogenic volatile organic compounds: oxidation, mechanisms, and organic aerosol, Atmos. Chem. Phys., 17, 2103-2162, 10.5194/acp-17-2103-2017, 2017.

Notholt, J., Hjorth, J., and Raes, F.: Formation of Hno2 on Aerosol Surfaces During Foggy Periods in the Presence of No and No2, Atmos. Env. A, 26, 211-217, 1992.

Oswald, R., Behrendt, T., Ermel, M., Wu, D., Su, H., Cheng, Y., Breuninger, C., Moravek, A., Mougin, E., Delon, C., Loubet, B., Pommerening-Roser, A., Sorgel, M., Poschl, U., Hoffmann, T., Andreae, M. O., Meixner, F. X., and Trebs, I.: HONO Emissions from Soil Bacteria as a Major Source of Atmospheric Reactive Nitrogen, Science, 341, 1233-1235, 10.1126/science.1242266, 2013.

Palm, B. B., Campuzano-Jost, P., Day, D. A., Ortega, A. M., Fry, J. L., Brown, S. S., Zarzana, K. J., Dube, W., Wagner, N. L., Draper, D. C., Kaser, L., Jud, W., Karl, T., Hansel, A., Gutierrez-Montes, C., and Jimenez, J. L.: Secondary organic aerosol formation from in situ OH, O-3, and NO3 oxidation of ambient forest air in an oxidation flow reactor, Atmos. Chem. Phys., 17, 5331-5354, 10.5194/acp-17-5331-2017, 2017.

Paul, D., Furgeson, A., and Osthoff, H. D.: Measurements of total peroxy and alkyl nitrate abundances in laboratory-generated gas samples by thermal dissociation cavity ring-down spectroscopy, Rev. Sci. Instrum., 80, Art. 114101, 10.1063/1.3258204 2009.

Paul, D., and Osthoff, H. D.: Absolute Measurements of Total Peroxy Nitrate Mixing Ratios by Thermal Dissociation Blue Diode Laser Cavity Ring-Down Spectroscopy, Anal. Chem., 82, 6695-6703, doi:10.1021/ac101441z, 2010.

Perring, A. E., Pusede, S. E., and Cohen, R. C.: An observational perspective on the atmospheric impacts of alkyl and multifunctional nitrates on ozone and secondary organic aerosol, Chem. Rev., 113, 5848-5870, doi:10.1021/cr300520x, 2013.

Peukert, S. L., Sivaramakrishnan, R., and Michael, J. V.: High temperature shock tube studies on the thermal decomposition of O_3 and the reaction of dimethyl carbonate with O-Atoms, J. Phys. Chem. A, 117, 3729-3738, doi:10.1021/jp400613p, 2013.

Pilegaard, K.: Processes regulating nitric oxide emissions from soils, Philos T R Soc B, 368, ARTN 20130126 10.1098/rstb.2013.0126, 2013.

Platt, U., Perner, D., and Patz, H. W.: Simultaneous Measurement of Atmospheric Ch2o, O3, and No2 by Differential Optical-Absorption, Journal of Geophysical Research-Oceans and Atmospheres, 84, 6329-6335, DOI 10.1029/JC084iC10p06329, 1979.

Pohler, D., Vogel, L., Friess, U., and Platt, U.: Observation of halogen species in the Amundsen Gulf, Arctic, by active long-path differential optical absorption spectroscopy, P Natl Acad Sci USA, 107, 6582-6587, 10.1073/pnas.0912231107, 2010.

Reed, C., Evans, M. J., Di Carlo, P., Lee, J. D., and Carpenter, L. J.: Interferences in photolytic NO2 measurements: explanation for an apparent missing oxidant?, Atmos Chem Phys, 16, 4707-4724, 10.5194/acp-16-4707-2016, 2016.

Roberts, J. M.: The atmospheric chemistry of organic nitrates, Atmos. Environ., Part A, 24, 243-287, 10.1016/0960-1686(90)90108-y, 1990.

Rollins, A. W., Browne, E. C., Min, K.-E., Pusede, S. E., Wooldridge, P. J., Gentner, D. R., Goldstein, A. H., Liu, S., Day, D. A., Russell, L. M., and Cohen, R. C.: Evidence for NOx Control over Nighttime SOA Formation, Science, 337, 1210-1212, 2012.

Romer Present, P. S., Zare, A., and Cohen, R. C.: The changing role of organic nitrates in the removal and transport of NOx, Atmos. Chem. Phys. Discuss., 2019, 1-18, 10.5194/acp-2019-471, 2019.

Romer, P. S., Duffey, K. C., Wooldridge, P. J., Allen, H. M., Ayres, B. R., Brown, S. S., Brune, W. H., Crounse, J. D., de Gouw, J., Draper, D. C., Feiner, P. A., Fry, J. L., Goldstein, A. H., Koss, A., Misztal, P. K., Nguyen, T. B., Olson, K., Teng, A. P., Wennberg, P. O., Wild, R. J., Zhang, L., and Cohen, R. C.: The lifetime of nitrogen oxides in an isoprene-dominated forest, Atmos. Chem. Phys., 16, 7623-7637, 10.5194/acp-16-7623-2016, 2016.

Rosen, R. S., Wood, E. C., Wooldridge, P. J., Thornton, J. A., Day, D. A., Kuster, W., Williams, E. J., Jobson, B. T., and Cohen, R. C.: Observations of total alkyl nitrates during Texas Air Quality Study 2000: Implications for O_3 and alkyl nitrate photochemistry, J. Geophys. Res. -Atmos., 109, Art. Nr D07303, doi:10.1029/2003jd004227, 2004.

Sadanaga, Y., Takaji, R., Ishiyama, A., Nakajima, K., Matsuki, A., and Bandow, H.: Thermal dissociation cavity attenuated phase shift spectroscopy for continuous measurement of total peroxy and organic nitrates in the clean atmosphere, Rev. Sci. Instrum., 87, 10.1063/1.4958167, 2016.

5 Schlesinger, W. H., and Hartley, A. E.: A Global Budget for Atmospheric Nh3, Biogeochemistry, 15, 191-211, 1992.

Schuster, G., Labazan, I., and Crowley, J. N.: A cavity ring down / cavity enhanced absorption device for measurement of ambient NO_3 and N_2O_5, Atmos. Meas. Tech., 2, 1-13, 2009.

10 Shirahama, N., Moon, S. H., Choi, K. H., Enjoji, T., Kawano, S., Korai, Y., Tanoura, M., and Mochida, I.: Mechanistic study on adsorption and reduction of NO2 over activated carbon fibers, Carbon, 40, 2605-2611, Pii S0008-6223(02)00190-2
Doi 10.1016/S0008-6223(02)00190-2, 2002.

Slusher, D. L., Huey, L. G., Tanner, D. J., Chen, G., Davis, D. D., Buhr, M., Nowak, J. B., Eisele, F. L., Kosciuch, E., Mauldin, R. L., Lefer,
15 B. L., Shetter, R. E., and Dibb, J. E.: Measurements of pernitric acid at the South Pole during ISCAT 2000, Geophys. Res. Lett., 29, Art. 2011, doi:10.1029/2002gl015703, 2002.

Sobanski, N., Schuladen, J., Schuster, G., Lelieveld, J., and Crowley, J. N.: A five-channel cavity ring-down spectrometer for the detection of NO_2, NO_3, N_2O_5, total peroxy nitrates and total alkyl nitrates, Atmos. Meas. Tech., 9, 5103-5118, 10.5194/amt-9-5103-2016, 2016.
20
Sobanski, N., Thieser, J., Schuladen, J., Sauvage, C., Song, W., Williams, J., lelieveld, J., and Crowley, J. N.: Day- and Night-time Formation of Organic Nitrates at a Forested Mountain-site in South West Germany, Atmos. Chem. Phys., 17, 4115-4130, 2017.

Su, H., Cheng, Y. F., Oswald, R., Behrendt, T., Trebs, I., Meixner, F. X., Andreae, M. O., Cheng, P., Zhang, Y., and Poschl, U.: Soil Nitrite
25 as a Source of Atmospheric HONO and OH Radicals, Science, 333, 1616-1618, 10.1126/science.1207687, 2011.

Tadic, I., Crowley, J. N., Dienhart, D., Eger, P., Harder, H., Hottmann, B., Martinez, M., Parchatka, U., Paris, J. D., Pozzer, A., Rohloff, R., Schuladen, J., Shenolikar, J., Tauer, S., Lelieveld, J., and Fischer, H.: Net ozone production and its relationship to NOx and VOCs in the marine boundary layer around the Arabian Peninsula, Atmos. Chem. Phys. Discuss., 2019, 1-35, 10.5194/acp-2019-1031, 2019.
30
Talukdar, R. K., Burkholder, J. B., Schmoltner, A. M., Roberts, J. M., Wilson, R. R., and Ravishankara, A. R.: Investigation of the loss processes for peroxyacetyl nitrate in the atmosphere: UV photolysis and reaction with OH, J. Geophys. Res. -Atmos., 100, 14163-14173, doi:10.1029/95jd00545, 1995.

35 Talukdar, R. K., Herndon, S. C., Burkholder, J. B., Roberts, J. M., and Ravishankara, A. R.: Atmospheric fate of several alkyl nitrates .1. Rate coefficients of the reactions alkyl nitrates with isotopically labelled hydroxyl radicals, Journal of the Chemical Society-Faraday Transactions, 93, 2787-2796, 1997.

Tang, M. J., Cox, R. A., and Kalberer, M.: Compilation and evaluation of gas phase diffusion coefficients of reactive trace gases in the
40 atmosphere: volume 1. Inorganic compounds, Atmos. Chem. Phys., 14, 9233-9247, 10.5194/acp-14-9233-2014, 2014.

Thieser, J., Schuster, G., Phillips, G. J., Reiffs, A., Parchatka, U., Pöhler, D., Lelieveld, J., and Crowley, J. N.: A two-channel, thermal dissociation cavity-ringdown spectrometer for the detection of ambient NO_2, RO_2NO_2 and $RONO_2$, Atmos. Meas. Tech., 9, 553-576, 10.5194/amt-9-553-2016, 2016.
45
Tingey, D. T., Manning, M., Grothaus, L. C., and Burns, W. F.: Influence of Light and Temperature on Isoprene Emission Rates from Live Oak, Physiol. Plant., 47, 112-118, DOI 10.1111/j.1399-3054.1979.tb03200.x, 1979.

Vandaele, A. C., Hermans, C., Fally, S., Carleer, M., Colin, R., Merienne, M. F., Jenouvrier, A., and Coquart, B.: High-resolution Fourier
50 transform measurement of the NO2 visible and near-infrared absorption cross sections: Temperature and pressure effects, J. Geophys. Res. -Atmos., 107, Art. 4348, 10.1029/2001JD000971, 2002.

von der Weiden, S. L., Drewnick, F., and Borrmann, S.: Particle Loss Calculator - a new software tool for the assessment of the performance of aerosol inlet systems, Atmos. Meas. Tech., 2, 479-494, DOI 10.5194/amt-2-479-2009, 2009.
55

Wang, S. S., Nan, J. L., Shi, C. Z., Fu, Q. Y., Gao, S., Wang, D. F., Cui, H. X., Saiz-Lopez, A., and Zhou, B.: Atmospheric ammonia and its impacts on regional air quality over the megacity of Shanghai, China, Sci Rep-Uk, 5, ARTN 15842 10.1038/srep15842, 2015.

5   Wild, R. J., Edwards, P. M., Dube, W. P., Baumann, K., Edgerton, E. S., Quinn, P. K., Roberts, J. M., Rollins, A. W., Veres, P. R., Warneke, C., Williams, E. J., Yuan, B., and Brown, S. S.: A measurement of total reactive nitrogen, NO_y, together with NO_2, NO, and O_3 via cavity ring-down spectroscopy, Env. Sci. Tech., 48, 9609-9615, doi:10.1021/es501896w, 2014.

Williams, E. J., Baumann, K., Roberts, J. M., Bertman, S. B., Norton, R. B., Fehsenfeld, F. C., Springston, S. R., Nunnermacker, L. J.,
10   Newman, L., Olszyna, K., Meagher, J., Hartsell, B., Edgerton, E., Pearson, J. R., and Rodgers, M. O.: Intercomparison of ground-based NO_y measurement techniques, J Geophys Res-Atmos, 103, 22261-22280, Doi 10.1029/98jd00074, 1998.

Womack, C. C., Neuman, J. A., Veres, P. R., Eilerman, S. J., Brock, C. A., Decker, Z. C. J., Zarzana, K. J., Dube, W. P., Wild, R. J., Wooldridge, P. J., Cohen, R. C., and Brown, S. S.: Evaluation of the accuracy of thermal dissociation CRDS and LIF techniques for
15   atmospheric measurement of reactive nitrogen species, Atmos. Meas. Tech. Discuss., 2016, 1-30, 10.5194/amt-2016-398, 2016.

Wooldridge, P. J., Perring, A. E., Bertram, T. H., Flocke, F. M., Roberts, J. M., Singh, H. B., Huey, L. G., Thornton, J. A., Wolfe, G. M., Murphy, J. G., Fry, J. L., Rollins, A. W., LaFranchi, B. W., and Cohen, R. C.: Total Peroxy Nitrates (ΣPNs) in the atmosphere: the Thermal Dissociation-Laser Induced Fluorescence (TD-LIF) technique and comparisons to speciated PAN measurements, Atmos. Meas. Tech., 3,
20   593-607, doi:10.5194/amt-3-593-2010, 2010.

Xu, L., Suresh, S., Guo, H., Weber, R. J., and Ng, N. L.: Aerosol characterization over the southeastern United States using high-resolution aerosol mass spectrometry: spatial and seasonal variation of aerosol composition and sources with a focus on organic nitrates, Atmos. Chem. Phys., 15, 7307-7336, 10.5194/acp-15-7307-2015, 2015.

Yamamoto, N., Kabeya, N., Onodera, M., Takahahi, S., Komori, Y., Nakazuka, E., and Shirai, T.: Seasonal-Variation of Atmospheric Ammonia and Particulate Ammonium Concentrations in the Urban Atmosphere of Yokohama over a 5-Year Period, Atmos Environ, 22, 2621-2623, Doi 10.1016/0004-6981(88)90498-2, 1988.

30   Yao, X. H., and Zhang, L. M.: Trends in atmospheric ammonia at urban, rural, and remote sites across North America, Atmos Chem Phys, 16, 11465-11475, 10.5194/acp-16-11465-2016, 2016.

York, D.: Least-Squares Fitting of a Straight Line, Can. J. Phys., 44, 1079-+, DOI 10.1139/p66-090, 1966.

35   Zare, A., Romer, P. S., Nguyen, T., Keutsch, F. N., Skog, K., and Cohen, R. C.: A comprehensive organic nitrate chemistry: insights into the lifetime of atmospheric organic nitrates, Atmos. Chem. Phys., 18, 15419-15436, 10.5194/acp-18-15419-2018, 2018.

Zasypkin, A. Y., Grigoreva, V. M., Korchak, V. N., and Gershenson, Y. M.: A formula for summing of kinetic resistances for mobile and stationary media: 1. Cylindrical reactor, Kinetics and Catalysis, 38, 772-781, 1997.
40

Zhang, W. J., Bagreev, A., and Rasouli, F.: Reaction of NO_2 with activated carbon at ambient temperature, Ind Eng Chem Res, 47, 4358-4362, 10.1021/ie800249s, 2008.
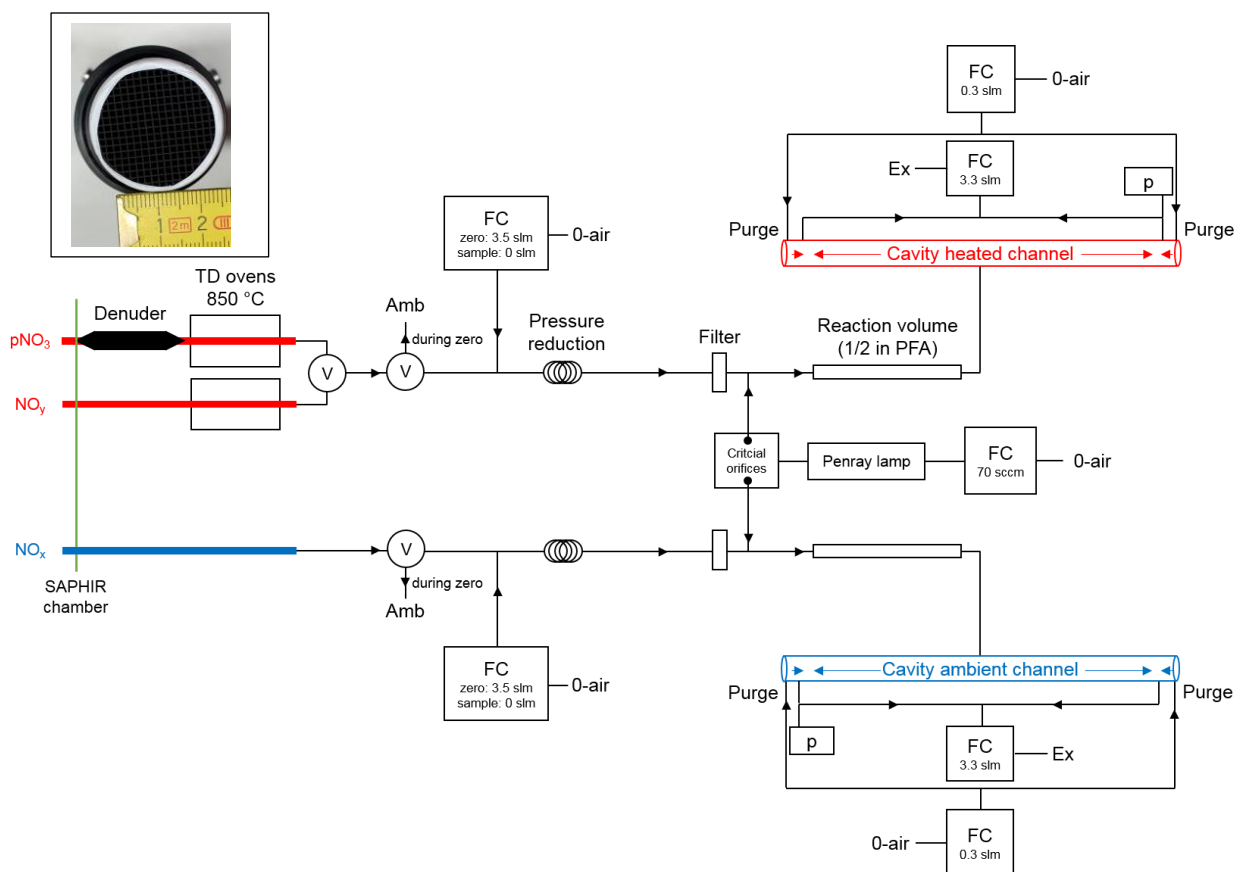
Figure 1: Schematic diagram of the TD-CRDS instrument. NO_y and pNit are detected via the heated channel, NO_x via the ambient channel. Ozone is generated via a Pen-Ray lamp (185 nm) and serves to convert NO to NO_2. TD = Thermal Dissociation, FC = flow controller. The flows listed are those used under normal operating conditions, p = pressure sensor, Ex = membrane pump and exhaust, Amb = ambient air outside of the chamber, V = electronically switchable valve. Filter = PTFE filter, 2 µm pore size). The inset (photo) shows the honeycomb structure of the activated carbon denuder.
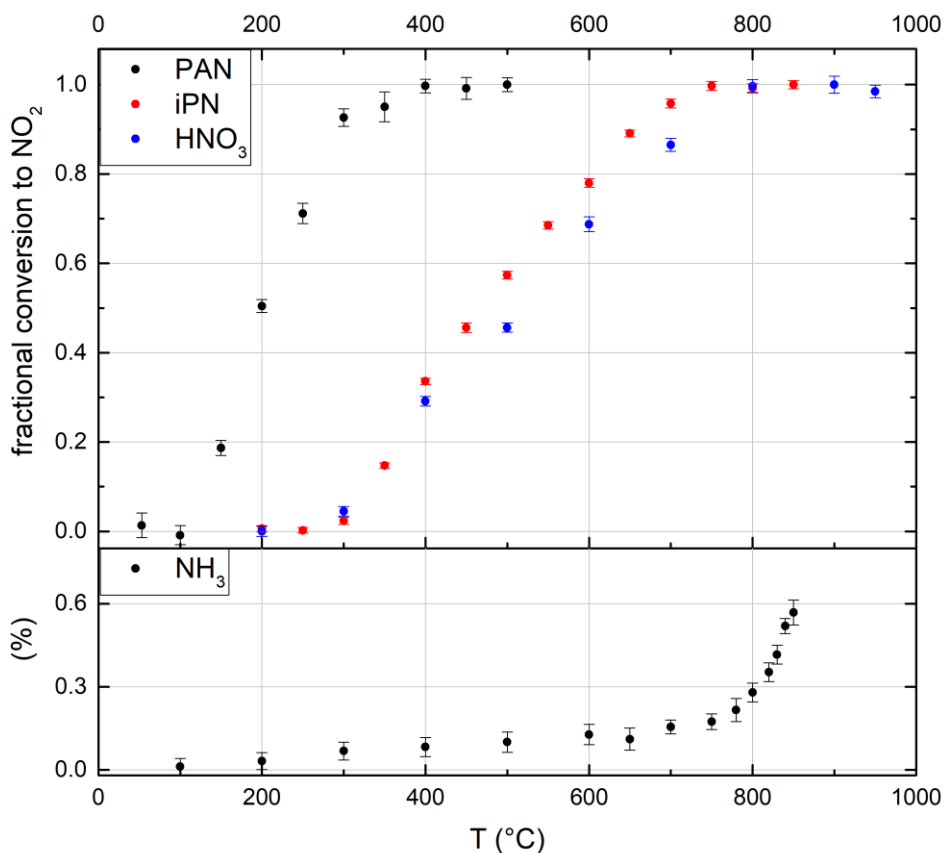
Figure 2: Thermograms of the NO_z species PAN, iPN, HNO_3 and the potential interference NH_3. The NH_3 fractional conversion is calculated relative to the calibrated output of the employed permeation source, all others relative to the observed mixing ratio at maximum conversion. Error bars are derived from the normed standard deviations during the averaging intervals. At the set temperature of 850 °C PAN, iPN and
5   HNO_3 are converted quantitatively to NO_2, while the NH_3 interference is negligible under common ambient conditions.
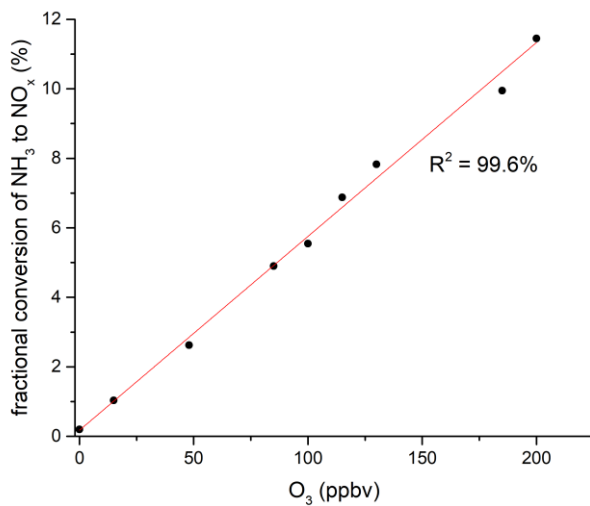
Figure 3: NH$_3$ to NO$_x$ conversion in the heated inlet channel of the instrument in the presence of O$_3$. The fractional conversion of NH$_3$ to NO$_X$ is calculated from the 13.1 ppmv of NH$_3$ from the permeation source.
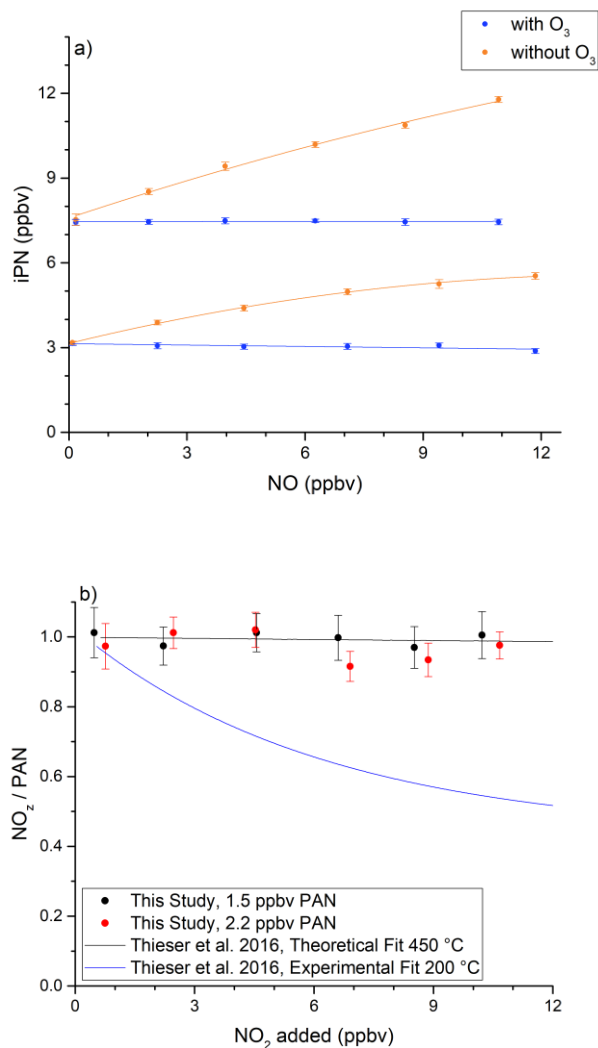
Figure 4: Investigation of bias caused by reactions of NO with HO_2 and RO_2 when measuring iPN. *a)* NO varied for two initial iPN mixing ratios in the presence (blue data points) and absence (orange data points) of added O_3. The NO_x background signal from the iPN cylinder was subtracted from the iPN mixing ratios. *b)* Investigation of bias caused by the recombination of RO_2 and NO_2 during the thermal decomposition of PAN. In both experiments the oven temperature was 850 °C. In both plots, the error bars indicate standard deviation over the averaging interval.
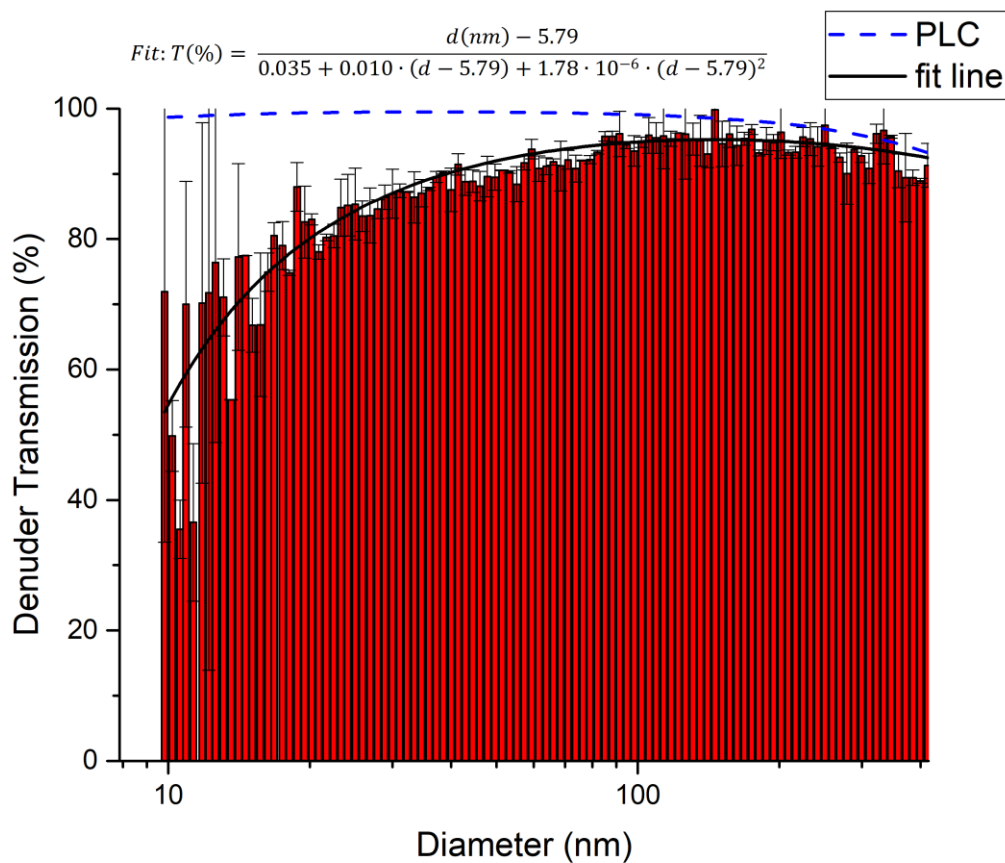
Figure 5: Transmission of ammonium nitrate particles through the denuder inlet. Relative transmissions are derived by dividing the number size distribution when sampling through the denuder by a size distribution obtained without the denuder. Error bars are based on the standard deviation of three consecutive measurements with and without the denuder. The plot also includes a fit of the experimental (solid, black line) data and a theoretical transmission distribution computed with the *Particle Loss Calculator (PCL)*.
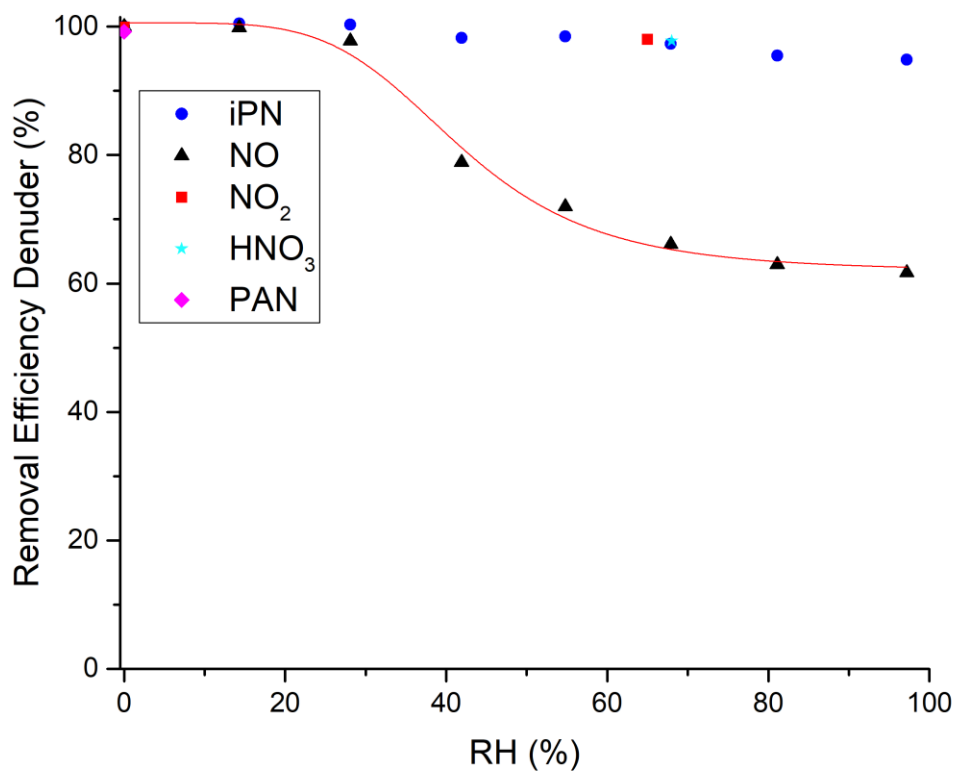
Figure 6: Removal efficiency of the denuder for various NO_y trace-gases as a function of RH.
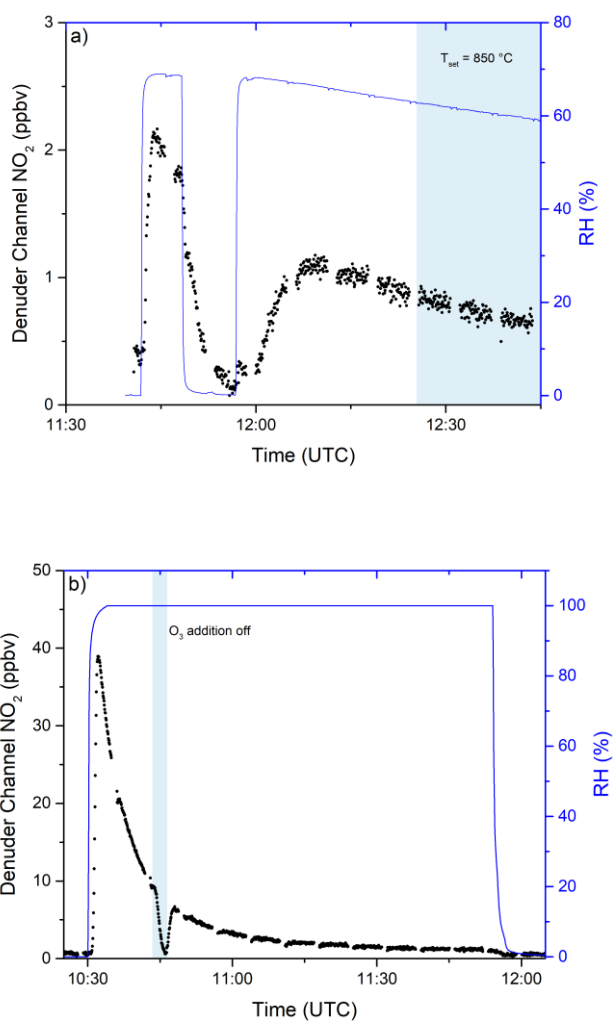
Figure 7: *a)* Release of NO_x from the denuder in humid air after exposure to 9.5 ppmv iPN for 1.5 hours. Relative humidity was measured before passing through the denuder. *b)* Release of NO_x from the denuder in humid air after exposure to 0.83 ppmv NO_2 for 4.8 days.
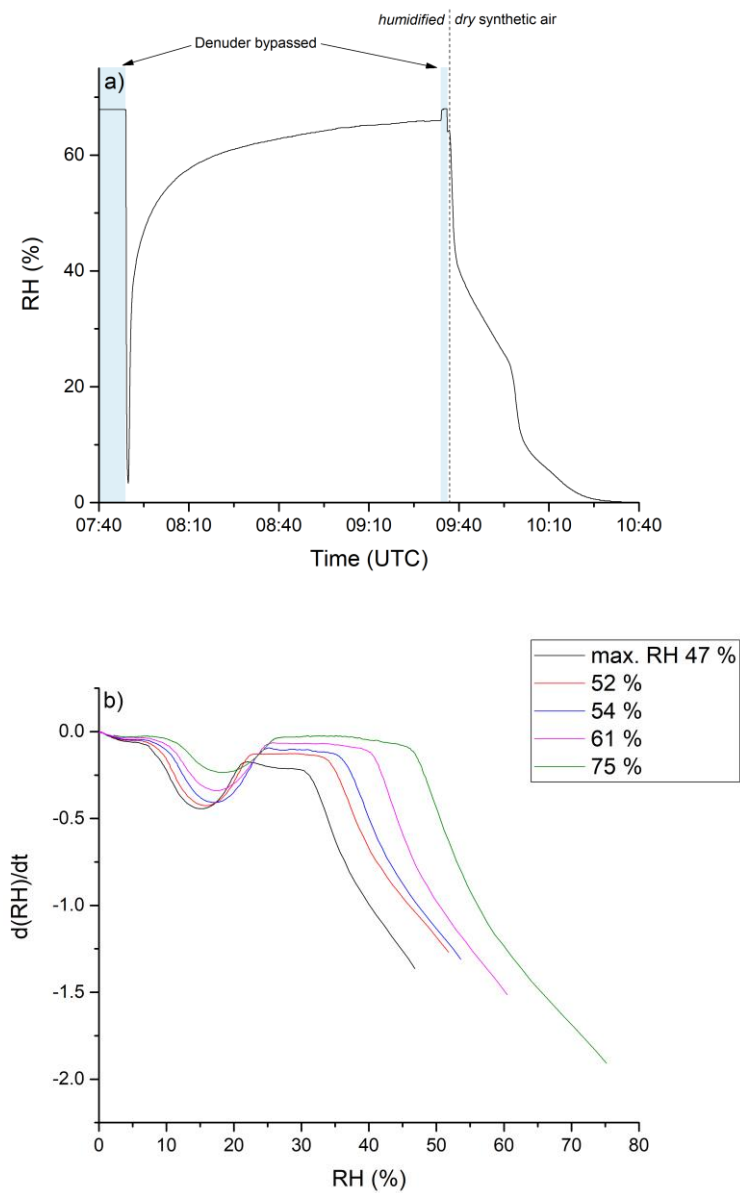
Figure 8: *a)* RH of humidified synthetic air after passing through the denuder. The initial RH was determined by bypassing the denuder before and after the experiment. *b)* Derivative of the measured RH during the drying period.
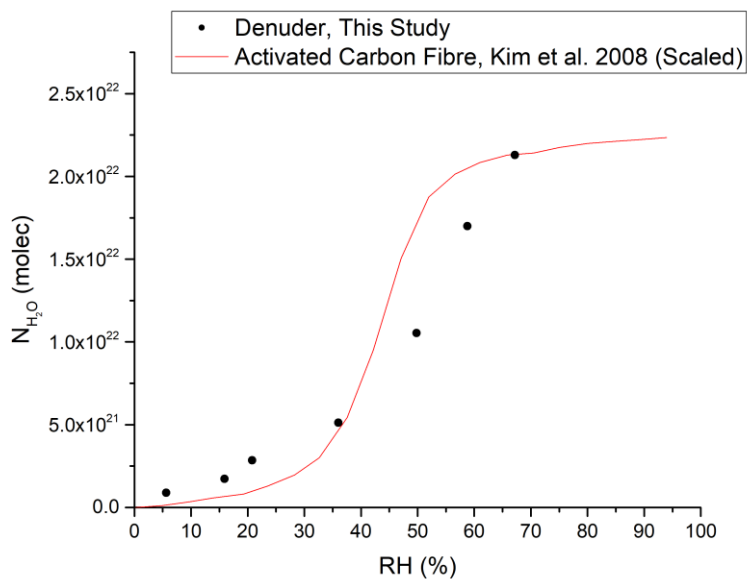
Figure 9: Number of adsorbed water molecules onto the denuder surface at equilibrium versus RH. The red line represents (scaled) results from a study on activated carbon fibre (Kim, P., Zheng, Y. J., and Agnihotri, S.: Adsorption equilibrium and kinetics of water vapor in carbon nanotubes and its comparison with activated carbon, Ind Eng Chem Res, 47, 3170-3178, 10.1021/ie0713240, 2008.).
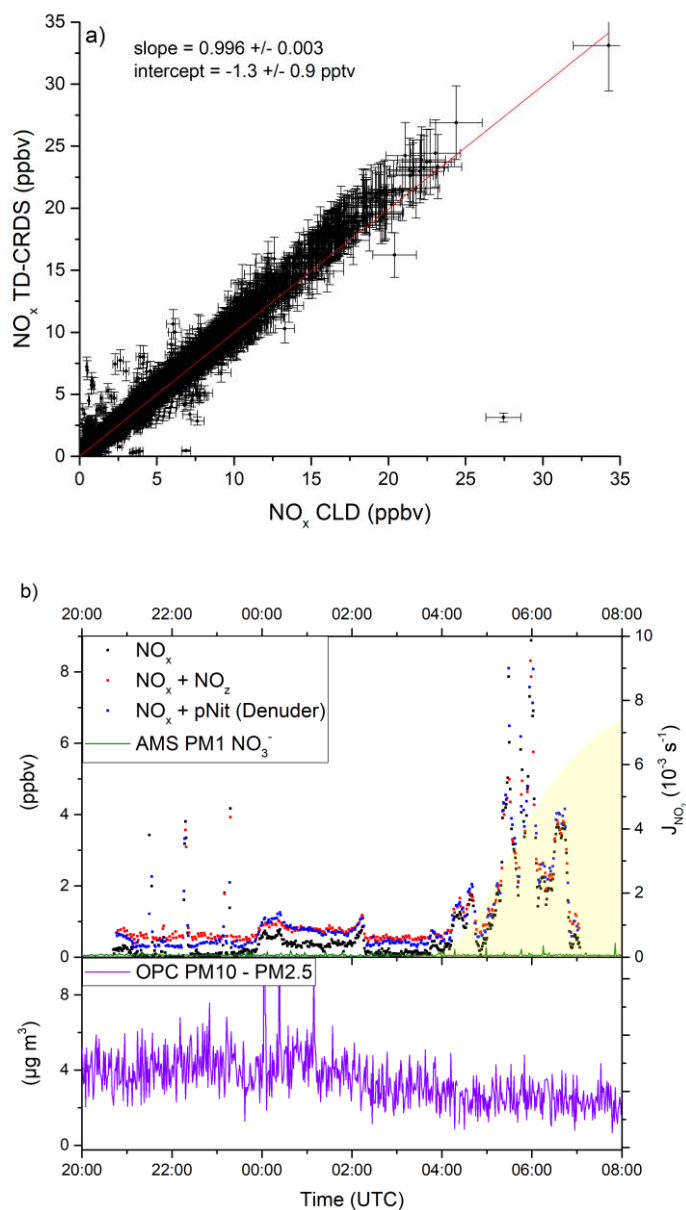
Figure 10: *a)* Correlation between the TD-CRDS NO_x measurements (1 min averages) and an independent CLD NO_x instrument from the
AQABA. Data obtained during phases of very high NO_x variability have been excluded (see Sect. 4.1). *b)* pNit measurements using the
denuder channel (blue data points) during AQABA and comparison with particulate NO_3^- from an AMS. The discrepancy towards the AMS
and the correlation with the NO_x mixing ratios indicate a positive bias in the pNit measurements, caused by humidity effects on the denuder
surface. OPC measurements are added in the lower panel to assess the potential influence of coarse mode aerosol nitrates.
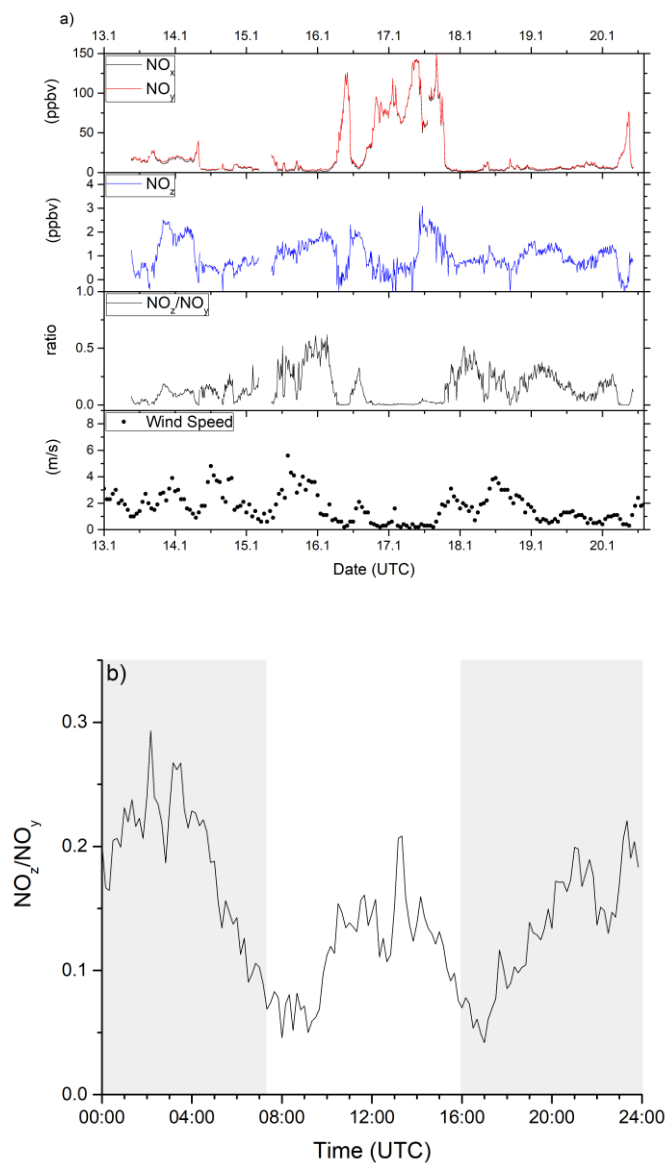
Figure 11: *a)* Time series of NO_x, NO_y, NO_z, NO_z/NO_y and wind speed from ambient measurements in Mainz, Germany in January 2020. Highly variable NO_x (between 0 and 150 ppbv) and moderate NO_z (between 0 and 3 ppbv) mixing ratios were observed, identifying the sampled air masses as dominated by anthropogenic emissions. Wind speed data was obtained from *Agrarmeteorologie Rheinland-Pfalz (*wetter.rlp.de) *b)* Diel profile of the NO_z/NO_y ratio including all measurement days, showing distinct minima during the morning and evening rush hours. Shaded areas signify the time between sunset and sunrise.